FINGERING INSTABILITY OF A GRAVITATIONALLY DRIVEN CONTACT LINE

JOHN MARK JERRETT, B.Sc.(Hons.)

FINGERING INSTABILITY OF A GRAVITATIONALLY DRIVEN CONTACT LINE

BY

© JOHN MARK JERRETT B.Sc.(Hons.)

A thesis submitted to the School of Graduate
Studies in partial fulfilment of the
requirements for the degree of
Master of Science

Department of Physics
Memorial University of Newfoundland

April 1992

St. John's Newfoundland

ISBN 0-315-73353-5

ABSTRACT

Presented here are the results of an experimental study of the flow of a viscous fluid sheet down a dry inclined plane. The three-phase contact line at the front of the flow is initially straight but becomes unstable to a roughly periodic variation in its downslope position when the sheet becomes thin enough. From measurements of the contact line position as a function of time for angles α in the range $0° < \alpha < 55°$, the flow is analyzed both before and after the instability occurs, and the development of the finger pattern is parameterized. These results are compared with those found in previous experiments and those predicted by theory.

ACKNOWLEDGEMENTS

I would like to thank my supervisor, Dr. John de Bruyn, for helpful advice, consultation, financial support and many proof readings of this thesis, the physics department for teaching assistantships throughout my masters program and Mr. Mike Ryan for the construction of my experimental apparatus.

TABLE OF CONTENTS

List of Figures

List of Tables

Chapter 1 Introduction

1.1 Introduction

The flow of a viscous fluid sheet down a dry inclined surface displays a common yet interesting instability. It is seen in paint flowing down a wall and rain running down a window pane. This instability is neither well understood theoretically nor thoroughly characterized experimentally.

Consider a volume of fluid uniformly distributed behind a gate at the upper end of a dry inclined surface. As the gate is opened, the fluid begins to flow down the slope with the contact line at the front of the flow being initially straight, as illustrated in Fig. 1-1. When the sheet thins to a certain fluid-dependent thickness, the contact line becomes unstable to a roughly periodic cross slope variation in its downslope position.[1] For certain fluid-solid combinations,[1,2] such as glycerin on a plexiglass surface, this variation grows into a series of rivulets or fingers of fairly uniform width (parallel sided fingers). These fingers continue to flow downhill while the upslope troughs between the fingers stop shortly after the instability develops. Thus the surface between the fingers remains dry and this pattern, shown in Fig.1-2, does not completely wet the surface.

For other fluid-solid combinations,[1] such as silicone oil on glass, the variation grows into a fairly periodic pattern of triangular shaped fingers (sawtooth pattern). In this case both the fingers and the troughs continue to flow downhill after the instability develops, although at different rates. This flow, shown in Fig. 1-3, will wet the entire surface.

These phenomena are important to many industrial processes where wetting by a thin film of fluid is required. Two examples are the spin coating of a magnetic

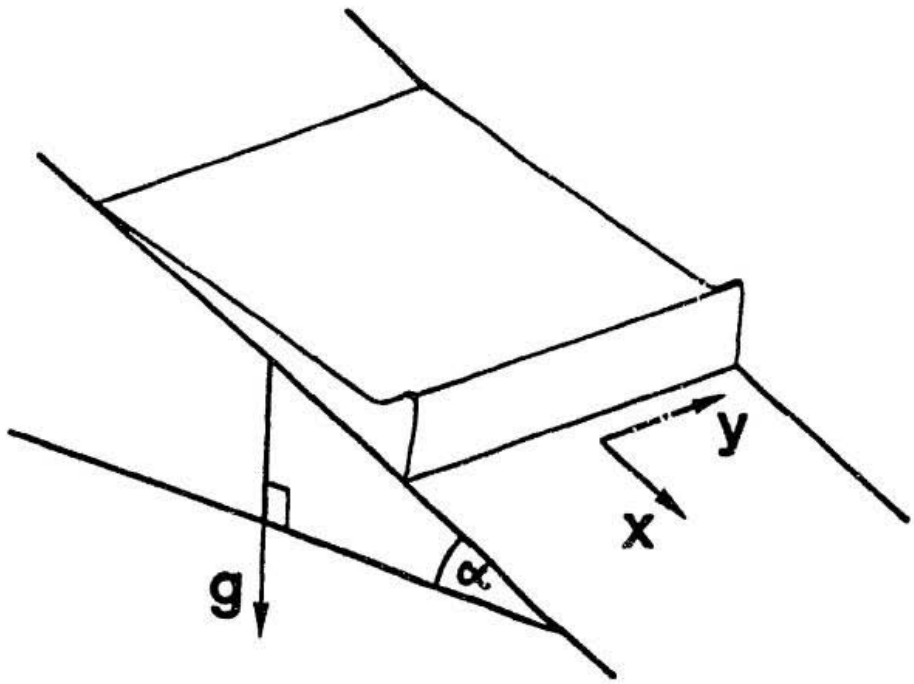

Fig. 1-1. A volume of fluid flowing down a dry, solid surface inclined at an angle α to the horizontal. Initially the contact line is straight as shown, but eventually it becomes unstable, developing fingers.

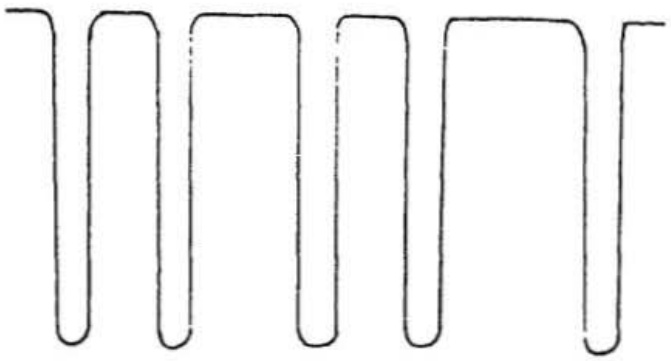

Fig. 1-2. Rivulet (parallel sided finger) pattern.

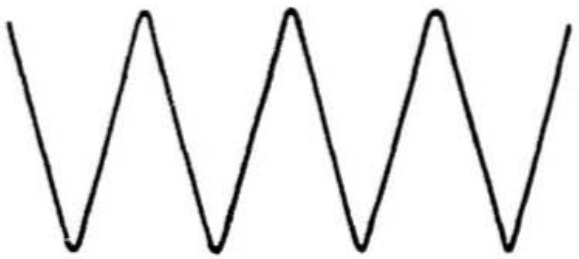

Fig. 1-3. Sawtooth pattern.

storage disk by a fluid initially placed at its axis of rotation and the lubricant coating on engine bearings. If the fluids used in these examples did not completely wet the surface undesirable 'dry patches' could form. For the above cases this would result in poor quality disks and engines which need frequent bearing replacement. In addition wetting phenomena and the physics behind them are of long standing interest both experimentally and theoretically[4,5] and have been well studied in both areas since the pioneering work of Young (1805)[6], Reynolds (1886)[7] and Rayleigh (1890).[8] Even with over one hundred years of study these phenomena are still not thoroughly understood.

1.2 Previous Work

The fingering instability of a moving contact line has been studied experimentally by Huppert[1] and Silvi and Dussan V.[2] A related instability, the fingering instability in the spreading of a rotating liquid drop, has been studied by Melo *et al.*[3]

Huppert studied this instability using a perspex surface and three fluids, namely glycerin and two silicone oils. He observed the rivulet pattern with glycerin, and the sawtooth pattern with both oils. He derived an expression for the position, x_n, of the stable contact line, neglecting surface tension, and found

$$x_n = (9A^{1/2} g \sin\alpha/4\mu)^{1/3} t^{1/3}, \qquad (1-1)$$

where A is the initial cross sectional area, μ is the viscosity and t is the time after release of the fluid. He also derived, including surface tension, an expression for the wavelength of the instability,

$$\lambda \propto (A^{1/2}\sigma/\rho g \sin\alpha)^{1/3}, \qquad (1-2)$$

where σ is the surface tension and ρ is the fluid density. He found that both Eqs. (1-1) and (1-2) agreed well with his experimental observations.

Silvi and Dussan V[2] studied the same instability using glycerin on both glass and plexiglass surfaces. They observed the rivulet pattern for glycerin on plexiglass, as did Huppert,[1] but found the sawtooth pattern for glycerin on glass. They measured the advancing contact angle to be 70° and 18° on plexiglass and glass respectively. Thus they concluded that the size of the advancing contact angle is an important factor in determining whether the rivulet or the sawtooth pattern will emerge for a given liquid-solid combination. They also found that their experimental observations were in agreement with Eq. (1–2) derived by Huppert.

Melo *et al.*[3] placed a drop of silicone oil at the axis of rotation of a silicon wafer. The liquid wetted the substrate, *i.e.*, the liquid-solid contact angle was zero. As the wafer was rotated, the drop spread out with an initially circular contact line. When the thickness of the fluid was small enough the contact line became unstable and fingers formed. While in this case the contact line was driven by centrifugal rather than gravitational force, the basic phenomena observed were similar to those described in the previous section.

In addition to the theoretical work of Huppert[1] mentioned briefly above, theoretical work on this instability has been carried out by Schwartz,[9] Hocking,[10] Goodwin and Homsy[12] and Troian *et al.*[13]

Schwartz[9] carried out numerical simulations using equations derived in the lubrication approximation and including surface tension. The advancing contact angle was taken to be zero, corresponding to a liquid which strongly wet the surface, and a no-slip boundary condition was applied at the edge of the flow corresponding to the experimental constraint of a wall. He found that the no-slip condition caused the contact line to be retarded at the edge of the flow. This perturbation initiated finger-

ing and the disturbance propagated inward along the contact line. He found that the longest finger is wedge shaped which is in agreement with experimental observations of wetting flows.

From scaling arguments and dimensional considerations he found that the wavelength should go like

$$\lambda \sim (\sin\alpha)^{-1/4} \qquad (1-3)$$

in contrast to the experimental and theoretical findings of Huppert[1] and the experimental results of Silvi and Dussan V[2] that $\lambda \sim (\sin\alpha)^{-1/3}$.

Without the no-slip boundary condition, small periodic perturbations imposed on the straight front eventually grew into fingers.

Neglecting surface tension caused the fingering phenomenon to disappear, both with and without the no-slip boundary condition. This seems to confirm Huppert's suggestion[1] that surface tension provides the destabilizing force.

Hocking[10] performed a linear stability analysis of a fluid *ridge* as opposed to a fluid sheet. One reason for selecting a fluid ridge comes from the experimental observation[3,11] of a bulge in the free surface of the fluid near the contact line when the fluid sheet is sufficiently elongated and the suggestion that the observed instability of the contact line is a result of the dynamics in this ridge. Another reason is, of course, to simplify the fluid sheet problem. Thus in studying a fluid ridge, Hocking hoped to simplify the problem while retaining the important dynamical processes. He found the ridge to be linearly unstable but not to fingers. Rather, the fluid tended to collect to one side of the channel and flow down the plane there. That is, he found the length scale of the instability to be dependent on the channel width in contrast to experimental observations.[1,2]

Hocking also considered the nonlinear development of the instability and presented preliminary numerical results that suggest the formation of a finger of fluid moving down the plane with a width that is independent of the channel width. He found no indication of the sawtooth pattern observed with some fluid-solid combinations and proposed that the sawtooth pattern is only a transient phenomenon which would eventually evolve into the rivulet pattern if the surface was long enough.

Goodwin and Homsy[12] have recently investigated the base state which develops prior to the instability using a combination of analysis and numerical solution. They showed that it is not possible to model the flow near the contact line in the lubrication approximation if a non-zero contact angle is imposed as a boundary condition, without requiring infinite velocities at the contact line. They derived and solved numerically Stokes flow equations for the region near the contact line with a contact angle boundary condition. They found the presence of a hump or bulge in the fluids free surface near the contact line as observed experimentally.[3,11] The magnitude of this bulge increased for increasing contact angle, increasing inclination angle and decreasing capillary number. The capillary number $Ca = \mu U/\sigma$ expresses the relative magnitude of viscous and surface tension forces; U is a characteristic velocity. They also observed a secondary bulge at large angles of inclination. They demonstrated that the bulge near the contact line arises from kinematic considerations and not from the contact line singularity. From their results they concluded that, except possibly at very small contact angles and small Ca, the lubrication approximations are not valid near the contact line.

Troian *et al.*[13] studied the lubrication equations with surface tension. They derived a form for the flow profile prior to the instability. This profile is a combination of an "outer" region, given by Hupperts' solution, Eq. 1-1, which ends abruptly at

$x = x_n$, and an "inner" region near the contact line which has a bulge, and which is smoothed by surface tension. Using scaling arguments, the inner and outer regions are matched, resulting in a flow profile similar to that observed experimentally. Then they matched this solution to a thin precursor wetting film. This was done to remove the contact line singularity, discussed further in chapter 2. A linear stability analysis was then performed on the resulting profile. They analysed the growth of imposed periodic perturbations over a range of wavenumbers and found the front to be unstable to wavenumbers $q \lesssim .9l$ with a maximum growth rate for a wavelength of $\lambda = 14l$. Here, $l = H/(3Ca)^{1/3}$ is the characteristic length over which surface tension competes with gravity and H is the film thickness.

1.3 Purpose and Scope

In this thesis I present measurements of the behaviour of the contact line both before and after the instability. The position of the contact line as a function of time was measured for three fluids on two surfaces with inclination angles in the range $0° < \alpha < 55°$. The flow was then analysed in terms of empirical fitting functions. The average wavelength of the instability and the width of the fingers were also studied.

This work was carried out in order to add to the experimental knowledge of the moving contact line. Measurements were made so as to characterize the motion of the contact line and the length scale of the instability which developed. My results, for the most part, confirm some theoretical predictions of the motion of the contact line and the length scale of the instability, while at the same time supplying new information about the finger width for which I have seen no experimental results or theoretical predictions. Most of my experimental observations agree with those of

others while one, the pattern produced by glycerin on glass, does not.

In Chapter 2 I will discuss some of the basic theory and terminology relevant to the study of dynamic contact lines, including wetting, contact angles, contact angle hysteresis, the contact line singularity, precursor films and the lubrication approximations. I will also discuss some of the previous theoretical treatments of the contact line instability in more detail. Chapter 3 will contain descriptions of the experimental apparatus used, the fluids and their relevent physical properties, the experimental procedure and the data gathering procedure. In Chapter 4 the experimental observations and results of fits of the data to empirical equations will be presented, while in Chapter 5 these results will be discussed and some theoretical explanations for the experimental observations will be presented. Chapter 6 will include the conclusions, and some possibilities for future experiments using the same apparatus will be presented.

Chapter 2 Theory

2.1 Introduction

The dynamics of moving contact lines are poorly understood. The usual theoretical approximations of fluid mechanics used to describe fluid flow break down at a contact line. It has been shown[14] that for a Newtonian, incompresible fluid with a no-slip boundary condition, unbounded forces result at the contact line. In the remainder of this thesis I will refer to the unbounded forces at the contact line as the "contact line singularity." Another problem involves the contact angle the fluid makes with the surface of the solid. It has been shown theoretically[5] and experimentally[15] that the observed or apparent contact angle may not be equal to the actual contact angle. The apparent contact angle may have a range of values for which the contact line does not move (contact angle hysteresis). A thin precursor film may preceed the macroscopically observable contact line resulting in the observable flow moving over a precoated, as opposed to dry, surface. The precursor film also causes confusion as to the positioning of the contact line in theoretical calculations.

2.2 Wetting Phenomenon

Young's equation,[6] which expresses the balance of horizontal forces at the static three-phase contact line of a solid-liquid-gas system, as shown in Fig. 2-1, states that

$$\gamma \cos\theta_e + \gamma_{sl} = \gamma_{sg}, \qquad (2-1)$$

where $\gamma = \gamma_{lg}$ is the interfacial tension between the liquid and gas, γ_{sl} between the liquid and solid and γ_{sg} between the solid and gas, and θ_e is the liquid-solid contact angle. The spreading parameter S is defined in the following way: an area of solid-gas interface has a surface free energy of γ_{sg} while the same area covered by a thick

coating of liquid has a surface free energy of $\gamma + \gamma_{sl}$. S is just the difference between these two surface free energies. S is written

$$S = \gamma_{sg} - \gamma_{sl} - \gamma \qquad (2-2)$$

$$= \gamma(\cos\theta_e - 1). \qquad (2-3)$$

When $S < 0$, *i.e.*, $\gamma_{sg} < \gamma + \gamma_{sl}$, the liquid does not spread; this corresponds to partial wetting. If $S \geq 0$ there is no balance of horizontal forces and complete wetting occurs. $S = 0$ corresponds to $\theta_e = 0$.

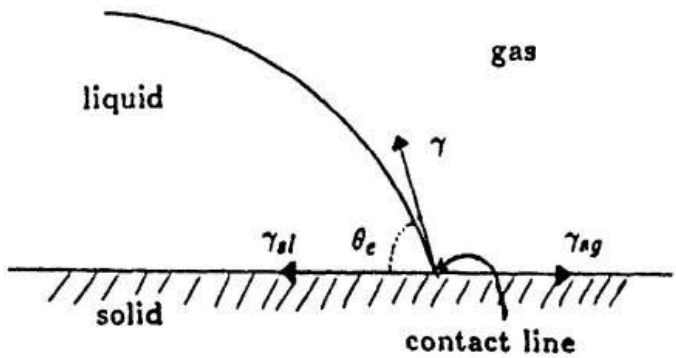

Fig. 2-1. Three phase contact line showing interfacial tensions γ, γ_{sl} and γ_{sg} and static contact angle θ_e.

In equilibrium vertical forces must also balance; these vertical forces can arise due to, for example, capillary forces and fluid weight.

2.3 Contact Angle Hysteresis

Figure 2-2 is a graph of contact angle versus contact line velocity for a typical fluid-solid system.

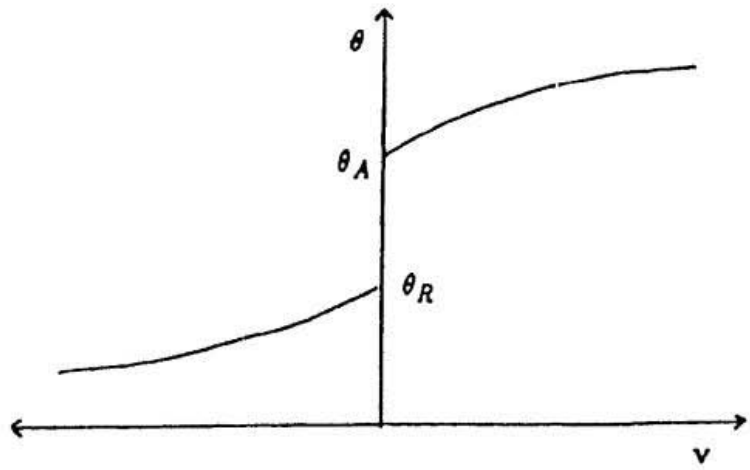

Fig. 2-2. The general form of the contact line angle θ at the solid-liquid contact line, as a function of contact line velocity.

For contact angles $\theta_R < \theta < \theta_A$ the contact line does not move, while it advances for $\theta > \theta_A$ and recedes for $\theta < \theta_R$. This phenomenon, whereby the contact line does not move even though the contact angle is varied from its equilibrium static value is known as contact angle hysteresis, and is very common. One experimentally verified cause of hysteresis is the microscopic roughness of the solid surface.[16,17] By coating a smooth solid surface with an organic monolayer, Zisman[16] found it unusual for θ_A and θ_R to differ whereas Dettre and Johnson,[17] using surfaces of increasing roughness, found that $\theta_A \neq \theta_R$, Fig. 2-3, for all surfaces.

Other possible causes of contact angle hysteresis are chemical contaminants or inhomogeneities in the solid surface and solutes in the liquid which may deposit a film on the surface. The surface condition plays an important role in wetting phenomena as it can affect the size of the liquid-solid contact angle,[16,17] and in the case of my

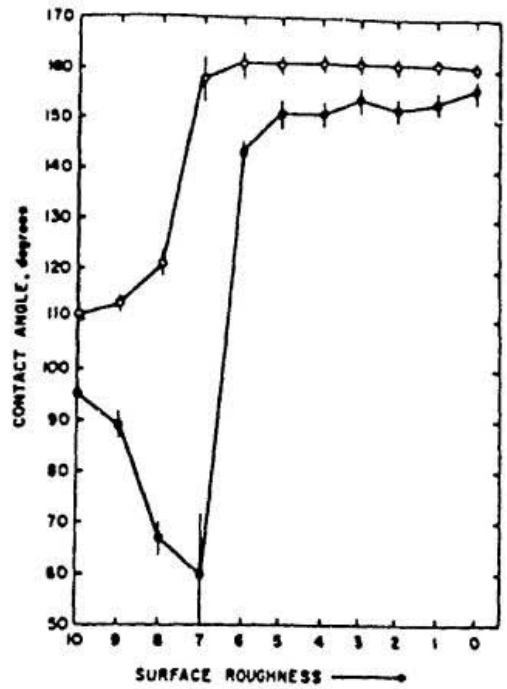

Fig. 2-3. Advancing and receding contact angles, θ_A and θ_R, as a function of surface roughness from reference 17.

experiments can thereby affect the pattern which develops from the instability.[2]

2.4 Contact Line Singularity

If a fluid moving along a solid surface is assumed to be Newtonian, incompressible and to obey the no-slip boundary condition, then unbounded forces will be produced at the contact line.[14] This singularity shows up in the lubrication approximations, to be discussed in section 2.6, by requiring a 90° contact angle between the liquid and solid. Since the lubrication approximations are used primarily for the spreading of thin films where the velocity vector is approximately parallel to the solid surface, obtaining a 90° contact angle implies that the lubrication approximations are not valid near the contact line. The singularity can be ignored if it is known that the fluid near the contact line does not affect the dynamics of the flow in the region of the

contact line and it can be removed by relaxing the no-slip boundary condition. The no-slip boundary condition is used simply because it removes the singularity but does not come from any physical understanding of the fluid flow near the contact line.[18]

2.5 Precursor Film

A fluid may advance on a dry substrate in two ways: 1] By a rolling motion, as shown in Fig. 2-4(a). 2] By means of a thin precursor wetting film which advances ahead of the observable contact lineas shown in Fig. 2-4(b). In the first case, the observable contact line is between the fluid and the dry surface, while in the second case it is between the observable fluid and an already wetted surface.

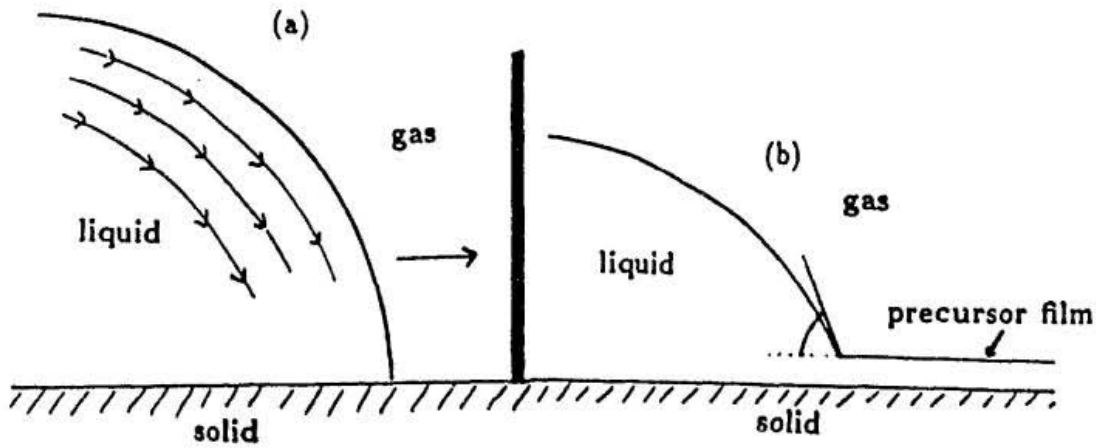

Fig. 2-4. Two possible methods of advance of a fluid film. Rolling motion (a) and advance over a precursor film (b).

Experiments indicate[14] that a drop of honey moving down an inclined glass surface tends to roll and not slide. The rolling motion was studied by placing a drop of dye on the surface of the honey and following the dye's motion as the honey moved. In my experiments the fluid also appeared to roll down the slope.

Experiments by Hardy[19] with drops of acetic acid on a horizontal glass surface (it was important that the air be dry) indicated that a precursor film was present beyond the observable contact line, even though the drops did not undergo any visible change in shape. He detected the film's presence by measuring a significant decrease in the value of the static friction of the surface. Drops of castor oil and paraffin on the same surface did not emit any measurable precursor film.[19]

Experiments were performed by Bascom *et al.*[20] using nonpolar fluids on clean, smooth metal surfaces in the presence of both saturated and unsaturated air. All the liquids used were chosen because they a macroscopically observable contact angle of zero degrees. They found that a precursor film was always present regardless of whether or not the air was saturated, the surface roughened or the liquids ultra purified, although these variables did affect the speed of advance of the film and whether or not the macroscopically observable body of fluid would spread over the precursor film. For example, squalane on stainless steel exhibited a precursor film approximately 20 Åin thickness as measured with an ellipsometer, and a leading edge which moved with speeds in the range 0.03 to 1.0 $\mu m/s$.

The precursor film may cause some confusion as to which leading edge, precursor or macroscopically observed, the contact line should be associated with.[5] If one chooses the precursor's leading edge, then the problem of the contact line singularity will be encountered and calculations involve a detailed analysis of a fluid with an unknown, anisotropic stress tensor. (The anisotropy is due entirely to the fluid's motion. A fluid at rest has an isotropic stress tensor.) An alternative choice would be to place the contact line at its observed position and model the precursor film as part of the surface.

2.6 Lubrication Approximations

In many theoretical treatments of the contact line instability, the fluid sheet can be modelled as a thin film and the lubrication approximations are used. These approximations allow a considerable simplification of the Navier-Stokes momentum equations. This discussion of the lubrication approximations follows that of Ref. (21).

The Navier-Stokes momentum equation for an incompressible Newtonian fluid in which the velocity is a continuous function of spatial coordinates is[21]

$$\rho \frac{D\vec{v}}{Dt} = -\nabla p + \mu \nabla^2 \vec{v}, \qquad (2-4)$$

where

$$\frac{D\vec{v}}{Dt} = \frac{\partial \vec{v}}{\partial t} + (\vec{v} \cdot \nabla)\vec{v}, \qquad (2-5)$$

the material derivative, accounts for spatial as well as time partial derivatives, ρ is the fluid density, p is the total pressure, μ is the shear viscosity and $\vec{v} = \hat{\imath}u + \hat{\jmath}v + \hat{k}w$ is the velocity. The pressure, p, could, as in the system studied in this thesis, include hydrostatic terms. We take the fluid sheet to lie in the x-y plane.

The Reynolds number, $Re = \rho U L/\mu$, expresses the relative magnitude of inertial and viscous forces. Here U is the surface velocity and L is the film breadth. For small Re, the time derivatives (or accelerations) are small compared with the viscous terms involving $\nabla^2\vec{v}$, and similarly for small Re the inertial terms $\rho(\vec{v} \cdot \nabla)\vec{v}$ are also negligible compared to the viscous terms. Applying the above simplifications to Eq. (2–4) gives the Stokes flow equations

$$\nabla p = \mu \nabla^2 \vec{v}. \qquad (2-6)$$

Further simplification of Eq. (2–6) can be made after putting it into dimensionless form by normalizing in-plane film velocities with respect to surface velocity U, vertical

velocity by $U\,h/L$, x and y distances with respect to film breadth L, z distances with respect to film thickness h and pressure with respect to ρU^2. w, the velocity in the z direction, is of order h/L smaller than u and v and can be neglected.[21] The normalized $\hat{i}$, $\hat{j}$ and $\hat{k}$ components of Eq. (2-6) then become

$$\frac{\partial p'}{\partial x'} = (\mu/\rho U L)\left(\frac{\partial^2 u'}{\partial x'^2} + \frac{\partial^2 u'}{\partial y'^2}\right) + (\mu L/\rho U h^2)\left(\frac{\partial^2 u'}{\partial z'^2}\right), \qquad (2-7a)$$
$$= \frac{1}{Re}\left(\frac{\partial^2 u'}{\partial x'^2} + \frac{\partial^2 u'}{\partial y'^2}\right) + \frac{1}{Re}\frac{L^2}{h^2}\left(\frac{\partial^2 u'}{\partial z'^2}\right),$$

$$\frac{\partial p'}{\partial y'} = (\mu/\rho U L)\left(\frac{\partial^2 v'}{\partial x'^2} + \frac{\partial^2 v'}{\partial y'^2}\right) + (\mu L/\rho U h^2)\left(\frac{\partial^2 v'}{\partial z'^2}\right), \qquad (2-7b)$$
$$= \frac{1}{Re}\left(\frac{\partial^2 v'}{\partial x'^2} + \frac{\partial^2 v'}{\partial y'^2}\right) + \frac{1}{Re}\frac{L^2}{h^2}\left(\frac{\partial^2 v'}{\partial z'^2}\right),$$

and

$$\frac{\partial p'}{\partial z'} = 0, \qquad (2-7c)$$

where primes indicate normalized quantities. Since $h \ll L$ and terms $\partial^2/\partial x'^2$, $\partial^2/\partial y'^2$ and $\partial^2/\partial z'^2$ are of the same order, then terms involving $\partial^2/\partial x'^2$ and $\partial^2/\partial y'^2$ in Eqs. (2-7) are much smaller than terms involving $\partial^2/\partial z'^2$. Applying these simplifications to Eqs. (2-7) and redimensionalizing results in the equations used in the lubrication approximation, namely

$$\nabla p = \mu\frac{\partial^2 \vec{v}}{\partial z^2}, \qquad (2-8a)$$

or, writing each component of Eq. (2-8a) explicitly,

$$\frac{\partial p}{\partial x} = \mu\frac{\partial^2 u}{\partial z^2} \qquad (2-8b)$$

for the $\hat{i}$ direction and

$$\frac{\partial p}{\partial y} = \mu\frac{\partial^2 v}{\partial z^2} \qquad (2-8c)$$

for the $\hat{j}$ direction with $p \approx p(x,y)$, $u = u(x,y,z)$ and $v = v(x,y,z)$.

2.7 Theoretical work of Reference 1

Huppert[1] used the lubrication approximations to analyze the flow of a thin, viscous fluid film before the contact line instability occured. In this section I rederive his results. It should be noted here that the lubrication approximation is valid only in the region away from the contact line since near the contact line film thickness and other quantities vary significantly over distances $\approx h$. Thus the approximations made in the last section are not valid near the contact line.

Assuming the free surface to be flat so that surface tension effects are negligible, and ignoring contact line effects, the pressure at a distance x down the slope due to the fluid in the film lying upslope of x is $p = -\rho g x \sin\alpha$. Thus $\partial p/\partial x = -\rho g \sin\alpha$ where α is the inclination angle and g is the acceleration due to gravity. Using the lubrication approximation, Eq. (2–8a), and the above expression for $\partial p/\partial x$, we find that the y-independent downslope momentum equation is

$$0 = \rho g \sin\alpha + \mu \frac{\partial^2 u}{\partial z^2}. \qquad (2-9)$$

Here, x is downslope coordinate, y is cross-slope coordinate and z is the coordinate normal to the surface. Following Huppert, the contact line effects can be neglected if the effect of surface tension is small compared to gravity effects, or more specifically, if the Bond number $B = \rho g L^2/\sigma \gg 1$, where σ is the surface tension and L is a characteristic length scale of the current. In the region where the free surface is not strongly curved, *i.e.*, away from the contact line, the contribution to the pressure in the fluid due to surface tension is negligible compared to the hydrostatic contribution. However, near the contact line the surface is significantly curved and the surface tension contribution is no longer negligible.

Using Eq. (2-9) and the boundary conditions $u = 0$ at $z = 0$ (the no-slip condition) and $\partial u/\partial z = 0$ at $z = h$ (tangential stress at the free surface must be zero), the fluid velocity as a function of height z in the fluid sheet is

$$u = (\rho g \sin\alpha/\mu)\left(h - \frac{z}{2}\right)z. \qquad (2-10)$$

The height averaged fluid velocity $\langle u \rangle$ is given by

$$\langle u \rangle = (\rho g \sin\alpha/\mu)\frac{h^2}{3}. \qquad (2-11)$$

The equation of continuity, $\partial\rho/\partial t + \nabla \cdot (\rho\vec{v}) = 0$, when averaged over the height of the fluid sheet, becomes

$$\frac{\partial h}{\partial t} + \frac{\partial}{\partial x}(h\langle u \rangle) = 0 \qquad (2-12)$$

for a fluid sheet of height $h(x,t)$. Substituting Eq. (2-11) into Eq. (2-12) gives the partial differential equation for the unknown free surface $h(x,t)$ to be

$$\frac{\partial h}{\partial t} + (\rho g \sin\alpha/\mu)h^2\frac{\partial h}{\partial x} = 0. \qquad (2-13)$$

From Eq. (2-13) we see that h is constant along characteristics given by

$$\frac{dx}{dt} = (\rho g \sin\alpha/\mu)h^2. \qquad (2-14)$$

If we let $h = f(x)$, for example, integration of Eq. (2-14) produces an equation for the characteristics

$$x = x_0 + (\rho g \sin\alpha/\mu)f^2(x_0)t, \qquad (2-15)$$

where x_0 is the initial value of the characteristic. Therefore the solution of Eq. (2-13) at long times is

$$h = [\mu(x - x_0)/\rho g \sin\alpha]^{1/2}t^{-1/2} \qquad (2-16a)$$

$$\simeq (\mu/\rho g \sin\alpha)^{1/2}x^{1/2}t^{-1/2} \qquad x \gg x_0, \qquad (2-16b)$$

where h in Eq. (2–16b) is independent of initial conditions. The equation expressing conservation of mass is

$$\int_0^{x_n(t)} h(x,t)\,dx = A, \qquad (2-17)$$

where x_n is the value of x at the front of the current and A is the initial cross-sectional area. From Eqs. (2–16b) and (2-17) we find that some time after the release of the fluid

$$0 \le x \le x_n = (9A^2\rho g \sin\alpha/4\mu)^{1/3} t^{1/3}. \qquad (2-18)$$

Thus Huppert predicts that the length of the film grows like $x_n \sim t^{1/3}$. By substitution of x_n from Eq. (2–18) into Eq. (2–16b) we find that the thickness of the fluid at the front of the film is

$$h_n = 3A/2x_n. \qquad (2-19)$$

Since, from Eq. (2–10), the fluid velocity increases with height, the solution of Eq. (2–13) will develop into a shock at large t. This unphysical result is due to the neglect of surface tension, which will tend to smooth the free surface profile near the flow front.

Huppert also derives an expression for the length scale of the contact line instability. He first finds the form of the quasi-steady two-dimensional fluid front by including surface tension and matching the tip onto the main flow given by Eq. (2-18). The addition to Eq. (2–13) of the terms due to surface tension leads to

$$\frac{\partial h}{\partial t} + (\rho g \sin\alpha/\mu)h^2\frac{\partial h}{\partial x} - (1/3)(\sigma/\mu)h^3\frac{\partial^4 h}{\partial x^4} = 0. \qquad (2-20)$$

Near the fluid front the dominant balance is between the gravitational and surface tension terms in Eq. (2–20), and thus

$$\rho g \sin\alpha \frac{\partial h}{\partial x} \approx (1/3)\sigma h \frac{\partial^4 h}{\partial x^4}. \qquad (2-21)$$

This gives

$$\frac{\partial h}{\partial x}\Big/\frac{\partial^4 h}{\partial x^4} \sim (\text{length})^3 \sim (\sigma h)/(\rho g \sin\alpha). \qquad (2-22)$$

Therefore a "typical" length scale is $\sim (\sigma h/\rho g \sin\alpha)^{1/3}$. Taking $h = h_n$ at the contact line gives a length scale for the contact line of $(\sigma h_n/\rho g \sin\alpha)^{1/3}$. Since the instability results from a competition between gravity and surface tension, it is reasonable to identify this length scale with the wavelength of the instability, and thus Huppert predicts that the wavelength of the instability varies like $(\sin\alpha)^{-1/3}$.

2.8 Theoretical work of Reference 13

Troian *et al.*[13] use Huppert's solution, Eq. (2-16b), which ends abruptly at $x = x_n$, Eq. (2-18), for the fluid profile far from the contact line (outer region). Then using the lubrication approximations with surface tension, the height profile, $h(x, y)$, is obtained from the solution of the height-averaged continuity equation

$$\frac{\partial h}{\partial t} + \nabla \cdot h\langle\vec{v}\rangle = 0. \qquad (2-23)$$

Here, $\langle\vec{v}\rangle = \langle u\rangle\hat{\imath} + \langle v\rangle\hat{\jmath}$ where $\langle u\rangle$ and $\langle v\rangle$ are height averaged velocities in the $\hat{\imath}$ and $\hat{\jmath}$ directions, respectively. They find a solution for the shape of the surface near the contact line and match this to Huppert's solution. In the lubrication approximation the velocity is given by

$$\mu\langle\vec{v}\rangle = (h^2/3)[\rho g \sin\alpha\hat{\imath} + \sigma\nabla\chi], \qquad (2-24)$$

where the curvature χ is given by $\chi \simeq (\partial^2 h/\partial x^2 + \partial^2 h/\partial y^2)$ in their approximation. In order to remove the contact line singularity (see section 2.4), they match the resultant fluid profile to a thin precursor film. They then perform a linear stability analysis of this solution and find it to be unstable to spatially periodic disturbances. I will now discuss their procedure in more detail.

For the unperturbed flow away from the contact line, the flow profile is given by Huppert's equations, Eq. (2-16b), which ends abruptly at x_n given by Eq. (2-18). Near the contact line (the "inner" region) the flow profile will be smoothed by surface tension. Troian *et al.* work in a reference frame moving with the contact line with velocity $U_0 = dx_n/dt$. To find the unperturbed profile in the inner region they write the profile as $h(x, y, t) = h_n(t)\, H(\xi, t)$ and require $H \to 1$ as $\xi = x/l \to \infty$ in order to match the solution ($h \sim h_n$) in the outer region. The dimensionless length $\xi = x/l$, where x is distance along $\hat{\imath}$ measured from the contact line and $l = h/(3\,Ca)^{1/3}$ is the characteristic length over which surface tension competes with gravity, where it is assumed that the capillary number $Ca = \mu U_0/\sigma \ll 1$. Assuming small Re, a time-independent solution of Eqs. (2-23) and (2-24) determines the function $H(\xi, t) = H_0(\xi)$.

The boundary conditions are first that for $\xi \to \infty$, the inner and outer solutions must match,*i.e.*, all derivatives of H with respect to x must vanish and $H_0 \to 1$, and second that near the contact line the dynamics must take into account the singularity due to the no-slip boundary condition ($\vec{v} = 0$ at $h = 0$). Troian *et al.*[13] remove this singularity by matching their flow profile to a thin precursor film of thickness $b\,h_n$, where $b \ll 1$. The equation they find for the flow profile is

$$H_0^2\left(1 - \frac{\partial^3 H_o}{\partial \xi^3}\right) = \frac{(1-b^3)}{(1-b)} - (1+b)\frac{b}{H}. \qquad (2-25)$$

The solution of Eq.(2-25) gives the profile shown in Fig. 2-5 for three values of b.

They then perform a linear stability analysis of the uniform profile to small perturbations in the $\hat{\jmath}$-direction, neglecting terms of order $b \ll 1$. They define $\zeta = y/l$ and look at perturbations with dimensionless wavevector $q = Q/l$. The position of

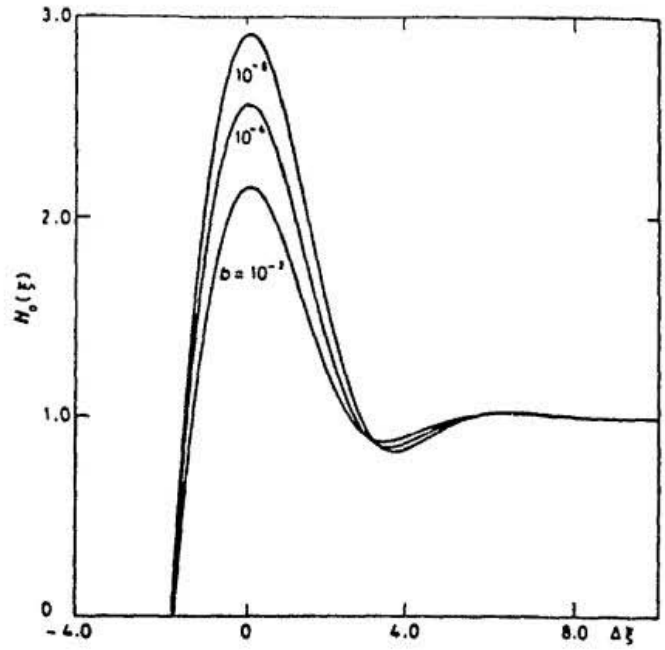

Fig. 2-5. Unperturbed flow profile calculated from Eq. (2-25) for three values of b as a function of $\Delta\xi$, which includes an arbitrary shift along the ξ direction so that the maxima line up. From reference 13.

the boundary is displaced from $\xi = 0$ to $\xi = \xi_B$, where

$$\xi_B(\zeta, t) = -A(\zeta)\, B(t). \qquad (2-26)$$

If $A(\zeta) = \cos(q\zeta)$, then the region $-\pi/2 < (q\zeta) < \pi/2$ is a section of the boundary perturbed in the forward x-direction, *i.e.*, a finger. The time-dependent amplitude of the perturbation is assumed to be of the form $B(t) = B_0 \cdot e^{\beta\tau}$ where $\tau = \int [U_0(t)/l]\, dt$ is proportional to the distance travelled. If $\beta > 0$, then $\partial B/\partial t > 0$ and the finger will grow.

Solving numerically the linearized continuity equation with the appropriate boundary conditions, Troian *et al.*[13] find the growth rate β to depend on the dimensionless wavenumber $q = Q/l$ and precursor film thickness b as shown in Fig. 2-6. Positive

values of β indicate unstable modes. The profile is unstable for $q \lesssim 0.9$ and even though there is a maximum growth rate for $\lambda = 14l$, a whole range of wavenumbers are unstable. This implies that the dominant wavelength for the instability will be $\lambda = 14l$, but perturbations with other wavelengths will also grow. This may explain why the experimentally observed instability is not perfectly periodic.[1,2]

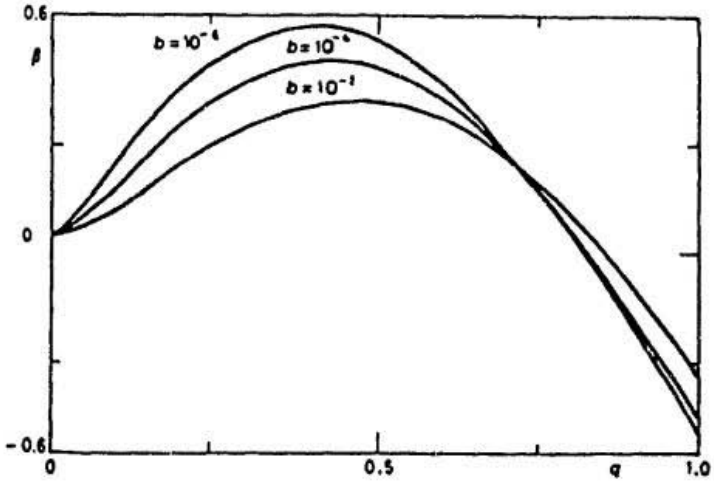

Fig. 2-6 β as a function of q, where positive values of β indicate unstable modes. From reference 13.

2.9 Theoretical work of Reference 12

Goodwin and Homsy[12] solve for the two-dimensional flow field and free surface shape in the vicinity of the contact line. They assume a slow moving, viscous Newtonian fluid advancing on a dry, inclined solid plane under the influence of gravity. They first recap Huppert's[1] work with the lubrication approximation neglecting surface tension and find that this results in a shock-type solution. In order to resolve this shock solution they include the first order effects of surface tension in the lubrication theory but obtain a different unphysical result. Then Goodwin and Homsy use a

different scaling in order to prescribe a contact angle boundary condition but find this results in an unrealistic contact line velocity. Finally they formulate a Stokes flow problem which permits satisfaction of a contact angle boundary condition. Allowing slip near the contact line removes the contact line singularity. They show that the inner region is governed by Stokes flow while in the outer region the flow is well described by lubrication theory.

Following the procedure of Huppert,[1] Goodwin and Homsy[12] calculate, in the lubrication approximation without surface tension, that the location of the leading edge prior to the instability goes like $x_n(t) \simeq (3/2)^{2/3} t^{1/3}$, with x scaled like $x \sim A/h^*$ where h^* is the characteristic length normal to the slope, and the thickness of the fluid at x_n is $h_n(t) \simeq (3/2)^{1/3} t^{-1/3}$, with h scaled by h^*. These equations are similar to Eqs. (2–16b) and (2–18) above derived by Huppert. Since surface tension was neglected, a shock-type solution is obtained with the front located at x_n.

Next they rescale the problem to include the first order effects of surface tension while retaining the lubrication approximations. They work in a reference frame moving with the average velocity of the contact line. They find the position of the free surface to be described by the differential equation

$$\left(1 + \frac{\partial^3 h}{\partial x^3}\right) h^2 = 1, \qquad (2-27)$$

subject to the boundary conditions $h = 0$ at $x = 0$, $h_x \to -\infty$ as $x \to 0$ and $h \to 1$ as $x \to -\infty$. In the limit $h \to 0$, the rate of change of curvature, $\partial^3 h/\partial x^3$, must be unbounded in order to satisfy Eq. (2–27). Since it is also required[5] that the slope of the free surface be unbounded at the contact line, a solution is not easily found.

Goodwin and Homsy found that a contact angle boundary condition could not be satisfied using either of the above cases, and so tried a new set of scalings which

would allow them to specify such a condition. They were also interested in how the no-slip condition affected their ability to model the flow near the contact line so a generalized slip boundary condition was introduced. Goodwin and Homsy again used the lubrication approximation including the first order effects of surface tension in a reference frame moving with the average velocity of the contact line.

The no-slip boundary condition was replaced by one in which the slip velocity is proportional to the product of the velocity gradient at the wall and a function, $S(h)$, of the fluid thickness. Following the same procedure as for the preceeding case, they find the differential equation for the shape of the free surface to be

$$\frac{\partial^3 h}{\partial x^3} = \frac{1 + S(h)}{S(h) \cdot h + h^2} - 1. \qquad (2-28)$$

The singularity at the origin can be removed by specifying $S(h) \sim O(h^{-1})$ as $h \to 0$. However, since $S(h)$ is proportional to the slip velocity, this introduces a singularity in the slip velocity.

The above three attempts to obtain a solution at the contact line using the lubrication approximations all contain a singularity. The singularity is either in the rate of change of curvature of the free surface with respect to position at the contact line for both the slip and no-slip models *or* in the slip velocity if a slip model is chosen. Thus they conclude that the lubrication approximations are of limited value in modelling the flow in the region of the contact line.

Finally, Goodwin and Homsy derive and solve numerically Stokes flow equations for the region near the contact line with a contact line boundary condition. The Stokes flow equations,

$$\nabla p = \mu \nabla^2 \vec{v}, \qquad (2-29)$$

are simplifications of the Navier-Stokes equations for a viscous fluid with very small Reynolds number. The pressure p in Eq. (2-29) includes gravity terms while Goodwin and Homsy write the gravitational terms separately. The Stokes flow equations differ from the lubrication equations in that $\nabla p = \partial p/\partial x\, \hat{i} + \partial p/\partial y\, \hat{j} + \partial p/\partial z\, \hat{k}$ and $\nabla^2 \vec{v} = \partial^2 \vec{v}/\partial x^2 + \partial^2 \vec{v}/\partial y^2 + \partial^2 \vec{v}/\partial z^2$ for Stokes flow, while in the lubrication approximation $\nabla p = \partial p/\partial x\, \hat{i} + \partial p/\partial y\, \hat{j}$ and $\nabla^2 \vec{v}$ is approximated by $\partial^2 \vec{v}/\partial z^2$. In this approximation an inner solution can be obtained. Goodwin and Homsy find solutions for the free surface profile over a range of capillary number, contact angle and inclination angle of $0.01 \leq Ca \leq 0.164$, $10° \leq \phi \leq 70°$ and $7.5° \leq \alpha \leq 135°$. As an example, Fig. 2-7 illustrates the calculated free surface shape for a contact angle of 70°, inclination angle of 45° and $Ca = 0.03$, 0.10 and 0.144 for curves a, b and c, respectively.

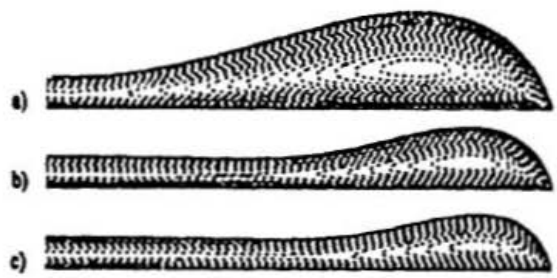

Fig. 2-7. Calculated flow profiles for a contact angle of 70°, inclination angle 45° and capillary numbers 0.03, 0.10 and 0.144 for profiles a, b and c, respectively. From reference 12.

Goodwin and Homsy find that near the contact line a hump or bulge of fluid occurs, the size of which increases with decreasing capillary number, increasing contact angle and increasing inclination angle. They demonstrate that the bulge is not due to the contact line singularity but is the result of an interaction between interfacial forces and and the stress field inside the fluid.

Chapter 3 Apparatus and Experimental Technique

3.1 Apparatus

The experimental apparatus is conceptually similar to that used by Huppert[1] and Silvi and Dussan V.[2] A sheet of plexiglass or glass $122cm$ in the downslope (x) direction, $91cm$ in the cross slope (y) direction and $1.3cm$ thick was clamped in a rigid aluminum frame. The angle of inclination α was adjustable; the measurements here were taken over a range of $0° < \alpha < 55°$. Graph paper with a grid of two inch squares marked on it was placed under the experimental surface to facilitate measurement of the contact line position. An aluminum gate spanning the full width of the surface was placed near the top of the slope. Foam rubber weather stripping was attached along the bottom of the gate to provide a seal to prevent leakage of the fluid prior to opening the gate. The seal also prevented the gate from scratching the surface. The gate was hinged at its upper end so that its axis of rotation was in the y direction and approximately $10cm$ above the surface. Thus when the gate was opened it swung out and up allowing the fluid to flow down the slope. An alternate method of opening the gate was to pull it directly up from the surface, but this usually resulted in jamming of the gate which in turn caused uneven release of the fluid.

The experiments were recorded using a Burle Industries CCD video camera connected to a video cassette recorder. The camera was mounted approximately $100cm$ to $125cm$ above and perpendicular to the surface. A $12.5mm$ focal length lens gave the camera a field of view wide enough to include the full width of the experimental surface. A Burle Industries video monitor was used to accurately position the camera, to watch each experiment from the camera's view point and to analyze the recorded experiments. A Laser 286/2L personal computer was employed for doing fits to the

data as discussed below.

3.2 Fluids

Experiments were carried out using three fluids: glycerin[22], 'heavy' mineral oil (HMO)[23] and 'light' mineral oil (LMO).[24] The density, viscosity, surface tension and static contact angle of each fluid were measured using the methods discussed below and are shown in Table I.

The first three of these are the physical properties of the fluids which enter into the theoretical treatments discussed in the previous chapter, and the fourth, as argued by Silvi and Dussan V[2], is important in determining the pattern that develops after the instability. The fluid properties of HMO and LMO are the same except for the viscosity, so a comparison of the flow development for these two fluids will show the effect, if any, of viscosity.

The density of each fluid was easily determined using a Mettler AE260 electronic balance having a resolution of $.0001\,g$. The mass of a known volume of fluid divided by its volume gave the density.

A Gilmont Instruments size 3 falling ball viscosimeter was used along with a stopwatch to measure each fluid's viscosity. The viscosimeter was filled with a fluid and the time of descent through a given height of a ball of known density was measured. The equation $\mu = K(\rho_b - \rho_f)t$ gave the viscosity in $(g/cm \cdot s) \cdot 10^{-2}$ (centipoise), where μ is the viscosity, K is a constant equal to $0.63cm^2/s^2$ for this viscosimeter, ρ_b and ρ_f are the densities in g/cm^3 of the ball and fluid respectively and t is the time of descent in seconds.

The surface tension was measured using a Cenco 70545 torsion wire tensiometer. This instrument consists of a torsion arm clamped to the middle of a torsion wire. A

Table I. Properties of fluids studied

	surface tension σ (dyn/cm)	viscosity μ (g/cm s)	density ρ (g/cm^3)	static contact angle [plexiglass] θ (degrees)	static contact angle [glass] θ (degrees)
Glycerin	59 ± 1	$11.1 \pm .1$	$1.26 \pm .01$	60 ± 2	50 ± 2
HMO	34 ± 1	$1.5 \pm .1$	$0.87 \pm .01$	14 ± 2	16 ± 2
LMO	32 ± 1	$0.5 \pm .1$	$0.85 \pm .01$	14 ± 2	16 ± 2

platinum-iridium wire ring of 5.992 cm circumference was connected to the other end of the torsion arm. After the instrument was calibrated with known masses, the ring was immersed in the fluid being measured. The torsion on the wire was increased and the fluid surface lowered simultaneously so that the torsion arm remained at its zero position. The scale reading was taken when the ring broke free of the fluid surface. From the calibration curve and a correction based on the fluid density the surface tension was calculated.

The static contact angle was measured by placing a drop of fluid on a horizontal piece of glass or plexiglass. The video camera was then positioned so that its optic axis was approximately aligned with the glass or plexiglass surface and the middle of the drop. Then a frame grabber, which was used to control the camera by computer, took a picture. From the printout of the picture the static contact angle was measured. An interesting observation concerning the static contact angle is that over a period of several hours it decreased. This decrease was small for HMO on both glass and plexiglass, for which it changed from $\sim 17°$ to $\sim 14°$ over 2 hours, but for glycerin on glass (plexiglass giving similar results) it went from $\sim 75°$ to $\sim 50°$ in 5 minutes, to $\sim 43°$ in 10 minutes and to $\sim 20°$ in 2.5 hours. This large change in the static contact angle for glycerin is due to the absorption by the glycerin of moisture from the air. During experiments, the fluid was left behind the gate for approximately 5 minutes and for this reason the value of the static contact angle for glycerin given in Table I is the value after 5 minutes exposed to the air.

3.3 Experimental Technique

All experiments were performed at room temperature which was not especially controlled and varied between 21 °C and 27 °C over the course of this work.

Before each experiment the solid surface was carefully cleaned to ensure uniform surface conditions. The cleaning procedure was as follows. After most of the fluid from a previous run had been removed, the surface was washed twice using detergent in water and rinsed each time with clean water. Then a commercial glass cleaner, Windex, was applied to the surface which was then wiped clean with paper towel or a chamois. Following this the surface dried quickly. Wiping the dry surface with dry paper towel created a static charge which had a dramatic and adverse effect on the flow; care was taken to avoid this.

Following the cleaning procedure, the surface was inclined to the appropriate angle and a level was used to make sure it was level in the y direction. The video camera was set perpendicular to the surface and positioned so that the gate was at the upper end of the video monitor screen. Then a known volume of fluid ($250cm^3$ for the experiments reported here) was poured behind the gate and left standing for a sufficiently long time that it was evenly distributed and stationary. Prior to opening the gate, the relevent parameters of the experiment such as the experimental surface, angle of inclination, type and amount of fluid and room temperature were recorded on the video tape. The camera was focussed on the surface, then the gate was opened and the fluid flowed down the slope with an initially straight contact line. Care was taking opening the gate so as to keep it straight and not allow one side to open before the other which would result in an uneven release of the fluid. It was also important not to open the gate too fast or the gate would throw drops of the fluid several centimeters down the clean surface. Since the fluids used were clear, only a shadow of the contact line could be seen. The curved surface of the fluid near the contact line caused the light passing through it to be refracted in such a way as to produce a shadow of the contact line on the grid below. In order to have only one

contact line shadow, only one set of ceiling lights was left on in the lab during each run. The lights were sufficiently far away so as to produce just one shadow. In a few later experiments with other fluids, a single light was placed in front of the slope. This produced a very distinct shadow of the contact line although fingers near the sides of the slope had their shadows displaced slightly giving the impression of a larger distance between the fingers. The actual fingers could be seen due to reflections from the finger tips, so this latter problem was easily overcome.

Experiments using HMO were performed over the ranges $2° \leq \alpha \leq 21°$ and $2° \leq \alpha \leq 20°$ for the plexiglass and glass surfaces respectively while the ranges for glycerin were $4° \leq \alpha \leq 30°$ and $4° \leq \alpha \leq 54°$ for the plexiglass and glass surfaces respectively. For inclination angles lower than the lower limit for each the contact line developed into poor fingers which tended to flow in the cross slope as well as the downslope directions and satisfactory measurements were not possible. For inclination angles larger than the upper limit for each the fluid would splash down over the surface much like a wave breaking on a beach, resulting in a nonuniform flow front.

3.4 Raw Data Gathering

The raw data was obtained by direct measurement of the contact line position from the video monitor during replay of a recorded experimental run. The position as a function of time of three or four fingers and troughs was measured for each run. The VCR used here incorporated a real-time counter so that the video tape could be moved ahead an appropriate number of seconds then stopped to take measurements. The zero time of each run was taken as the time at which the contact line shadow first appeared from under the opened gate. The finger and trough measurements started

at the point at which the contact line began to show the instability. Also measured were the distance downslope, x_n, at which the contact line became unstable, the finger width, δ, taken as the full width at half the finger length and the average wavelength, $\overline{\lambda}$, of the finger pattern. The fluid at the edges of the flow was held back by the walls at each edge of the surface causing the contact line to be curved in that area. For this reason the fingers closest to each edge were not included in the calculation of the average wavelength.

Chapter 4 Results

4.1 General Observations

Experiments with all three fluids were performed on the plexiglass surface, while only glycerin and HMO were used on the glass surface. In all cases the rivulet (parallel sided finger) pattern was observed. Since I took substantially more data for HMO than for LMO, I will quote only data for HMO except in cases were the LMO data is of importance although data for LMO is shown on some of the figures below. In the case of glycerin, the troughs appeared to stop shortly after the contact line became unstable while for HMO, the troughs continued to move very slowly downhill. The observed fingering pattern was not perfectly periodic, nor were the finger lengths perfectly uniform. Several preliminary experimental runs were tried with silicone oil on glass, for which the unstable contact line developed into the sawtooth pattern in which both the fingers and troughs continued to move downhill, but at different rates. In this case the fingering pattern was fairly periodic. The finger lengths were more uniform than for the rivulet pattern but still not perfectly uniform.

The fluid at the edges of the flow was held back by the walls at the edges of the surface. This perturbation of the contact line resulted in fingers forming at the edges. Although Schwartz[9] found numerically that this edge perturbation caused fingering as it propogated inward along the contact line, all experiments here indicate that the entire contact line becomes unstable simultaneously. Due to the surface's large width ($91cm$), any edge effects are expected to be small in the middle region of the surface.

4.2 Before the Instability

Huppert[1] predicted that, prior to the instability, the position of the uniform contact line should advance like $t^{1/3}$; his measurements agreed with this prediction.

Due to this, I analyzed my data from before the instability by fitting the position to a power law in time, *i.e.*,

$$x = A_0(t - t_0)^{\beta_0}. \qquad (4-1)$$

Fits to Eq. (4-1) were performed only for $\alpha \leq 14°$ for glycerin and $\alpha \leq 8°$ for HMO. At higher angles the time before the instability was too short for enough position measurements to be made and meaningful fits to Eq. (4-1) were not possible. The data was well described, for the most part, by Eq. (4-1) but the exponent β_0 was substantially larger than the value of 1/3 predicted by Huppert. In fact the exponents, shown as open symbols in Figs. 4-3, are in reasonably good agreement with the exponents characterizing the growth of the fingers which develop after the instability. similarly, the values of the amplitude A_0 of Eq. (4-1), shown as open symbols in Figs. 4-4, agree within error with the corresponding value for the flow after the instability.

Fits to data from two different runs having the same experimental parameters produced results which were equal within experimental error, thus indicating that the flow is reproducible.

The discrepency between my results and the $t^{1/3}$ behaviour found by Huppert can be understood from Fig. 4-1, which shows the front position as a function of time for HMO on plexiglass with $\alpha = 8°$, both before and after the instability. The pre-instability data, shown as open symbols, seems to approach a $t^{1/3}$ behaviour, but only after a transient period in which the front advances more quickly.

This behaviour is seen only at the smallest angles. At larger angles, $\alpha \gtrsim 5°$ for HMO and $\alpha \gtrsim 8°$ for glycerin, the instability occurs before the transient has relaxed and the approach to $t^{1/3}$ behaviour is not observed.

The film thickness at the onset of the instability was not measured quantitatively.

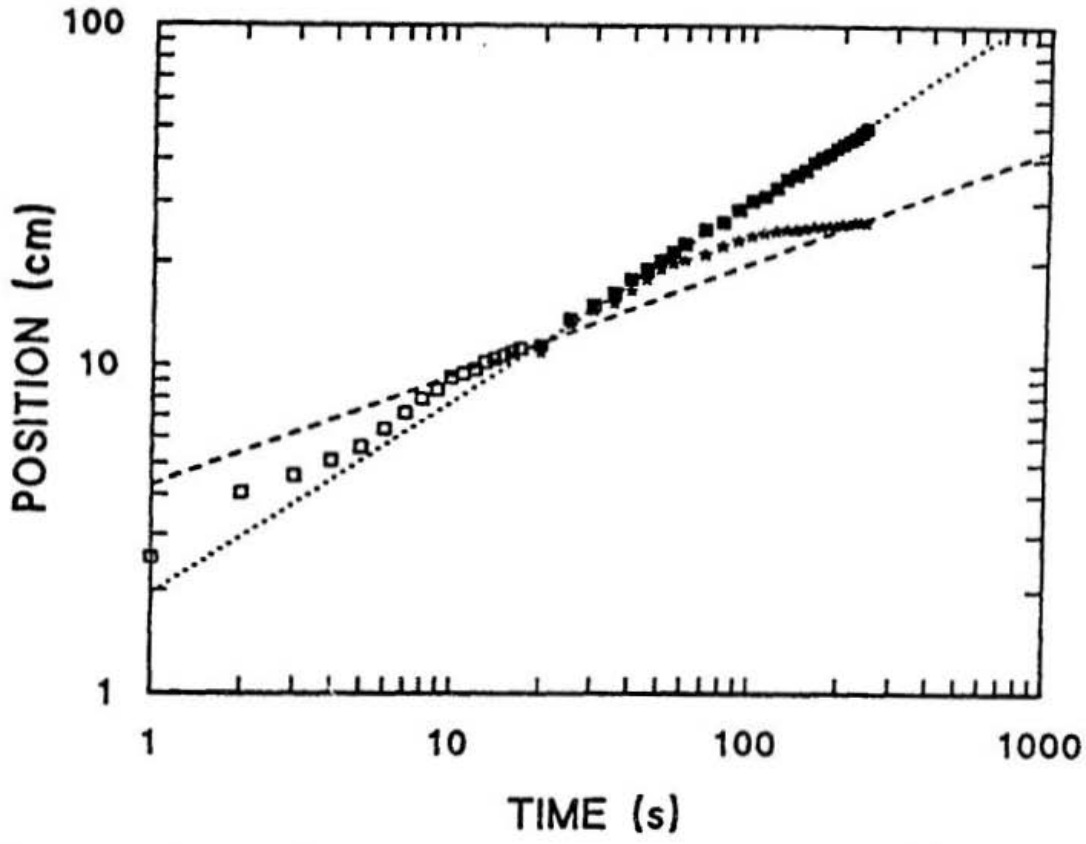

Fig. 4-1. Position *vs.* time for HMO on plexiglass at $\alpha = 3°$. The position of the uniform front before the instability (open squares) advances faster than $t^{1/3}$ at early times and appears to approach a $t^{1/3}$ growth (dashed line) at later times. The solid squares and stars show the finger tip and trough positions, respectively, after the instability, and the dotted line shows the power law growth of the finger tip position.

However rough estimates were made based on Huppert's result that the fluid thickness at the front of the shock solution, Eq. (2-18), is given by Eq. (2-19). My data for x_n suggest that the contact line becomes unstable when the fluid thins to a certain fluid-dependent thickness on the order of three millimeters. This critical thickness is $h_n \approx 0.33\,cm$ for glycerin and $h_n \approx 0.27\,cm$ for HMO.

4.3 After the Instability

Since I am unaware of any theoretical predictions for the growth of the developing fingers beyond the regime where linear stability analysis is valid,[25] I analyzed my data in terms of empirical fitting functions. The downslope tip position after the instability, x_d, was well described, within experimental error, for all fluids on both substrates at all angles α by a power law in time:

$$x_d = A(t - t_0)^{\beta}, \qquad (4-2)$$

where the amplitude A, the exponent β and the time origin t_0 were all used as free parameters. A typical fit to Eq. (4-2) is shown in Fig. 4-2 for HMO on plexiglass at 8°.

The trough position, x_u, was fitted to the function

$$x_u = B\,e^{t/\tau} + C\,t + D \qquad (4-3)$$

with B, C, D and τ as free parameters. A typical fit of this function to experimental data is also shown in Fig. 4-2.

Other fitting functions were tried but gave less satisfactory descriptions of the data. In particular, power law fits to the trough data were tried, but they gave satisfactory fits only when the troughs continued to moved with sufficiently high

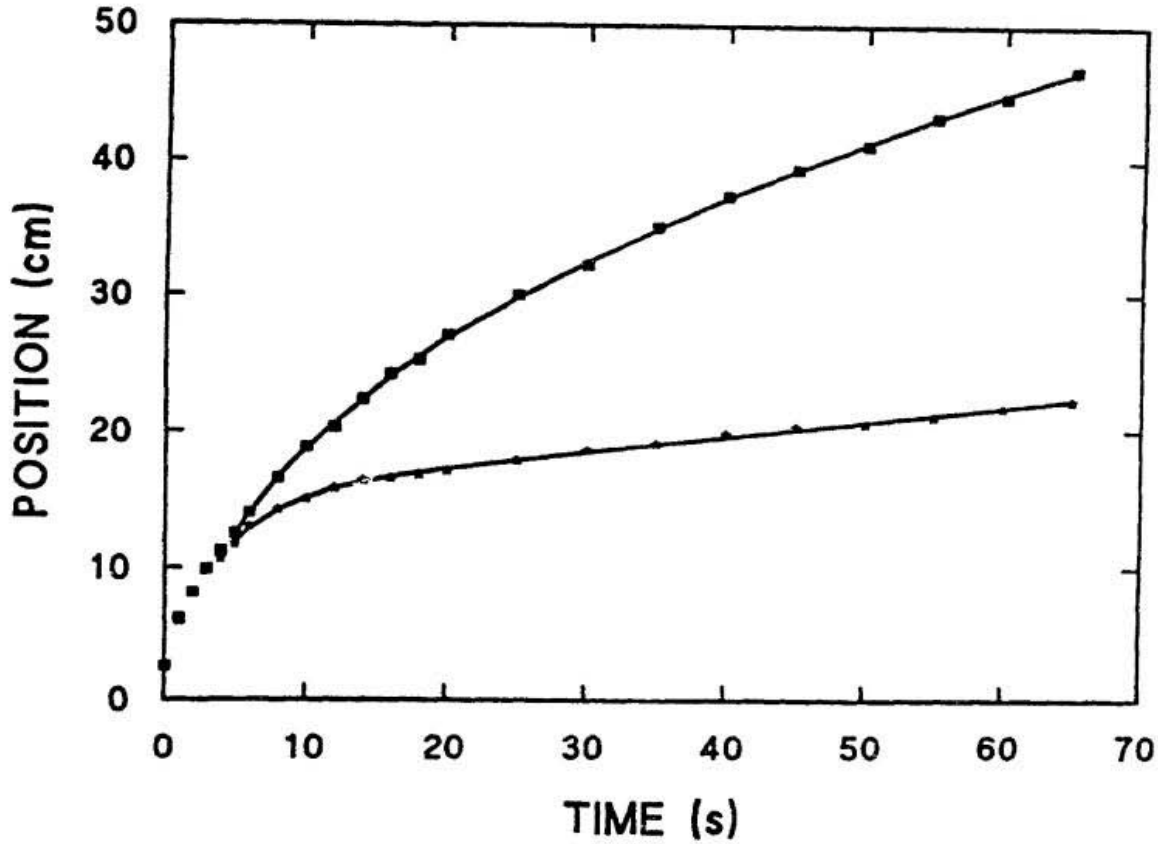

Fig. 4-2. The downslope position of two points on the contact line of a $250cm^3$ sample of HMO on plexiglass at $\alpha = 8°$. the squares correspond to a point which is at the tip of a finger after the instability occurs, and the stars to one in a trough. The lines are fits to Eqs. (4-2) and (4-3) for the finger and trough, respectively.

speeds, *e.g.*, the power law fit would not work for glycerin troughs but did work for some HMO troughs.

Figs. 4-3(a) to (d) show the tip growth exponent β as a function of $\sin\alpha$ for glycerin and both oils on plexiglass, (a) and (b), and for glycerin and HMO on glass, (c) and (d).

Each point on these plots (and similar plots below) represents the average of results from fits to a number (three for very low angles and four for other angles) of fingers (or troughs) from a particular run. The error bars represent the range of values obtained from all of the fits to that data set. The range of values obtained for different runs at the same angle is roughly the same indicating that any variability in surface condition between runs is no greater than the variability across the slope for a single run.

For both fluids, glycerin and HMO, on both substrates, β is essentially independent of α within experimental uncertainties. The mean value of β for the plexiglass surface is $0.65 \pm .04$ for glycerin and $0.52 \pm .05$ for HMO; for the glass surface $\beta = 0.55 \pm .05$ for glycerin and $0.48 \pm .01$ for HMO. (Errors here and elsewhere in this thesis are statistical standard deviations.) These values of β are also shown in Table II. My value for glycerin fingers on plexiglass is in agreement, within experimental error, with the exponent of .6 reported by Huppert[1]. β does show a slight tendency to decrease with increasing α for HMO on both surfaces and for glycerin on glass but it is difficult to tell if this trend is real from my data. The values of β and β_0, where values of β_0 are represented as open symbols in Figs. 4-3, appear to be equal within experimental uncertainty in most cases.

Figs. 4-4 show the dependence of finger growth amplitude A on α for plexiglass,

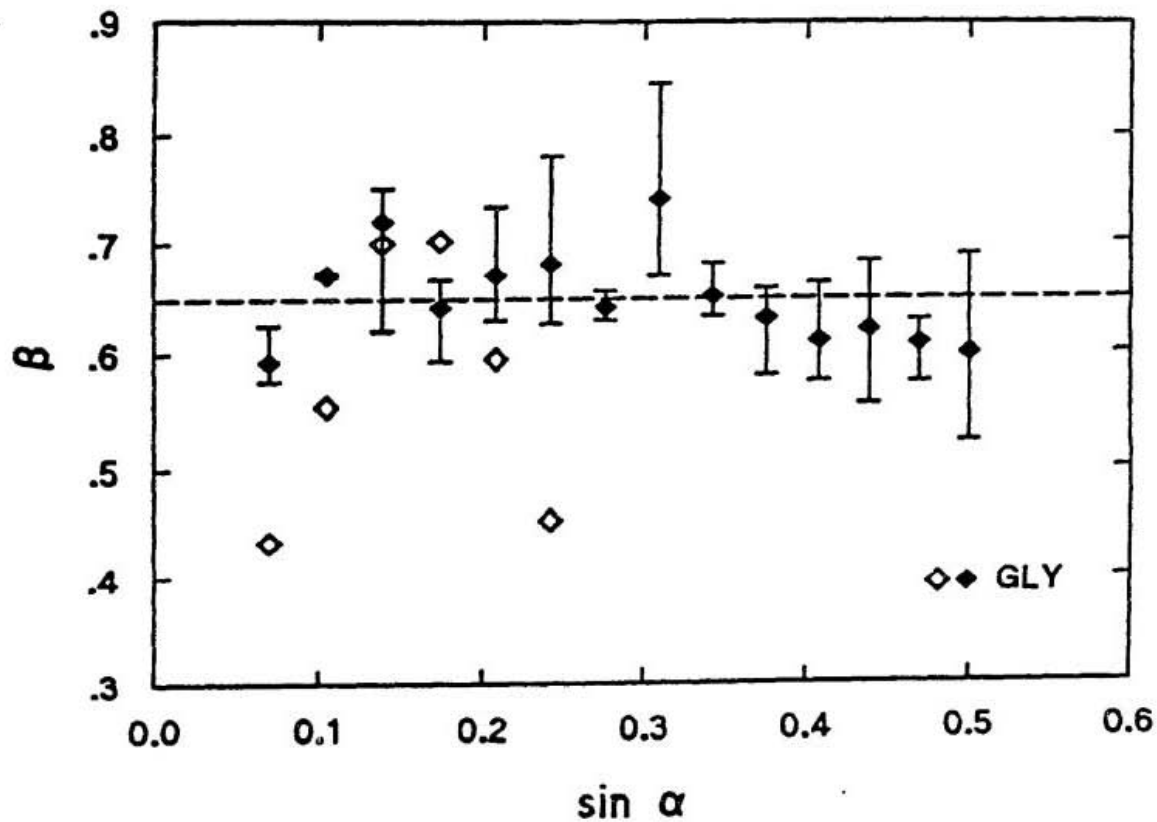

Fig. 4-3(a). The solid symbols show the exponent β of Eq. (4-2) as a function of $\sin\alpha$ for glycerin on plexiglass. The dashed lines show the average for each case. The data points indicate the mean values and the error bars the range from fits to several fingers at each angle. The open symbols show the exponent β_0 for the flow before the instability, determined from Eq. (4-1). For clarity, error bars for these points are not shown; they are similiar in size to those for the other data.

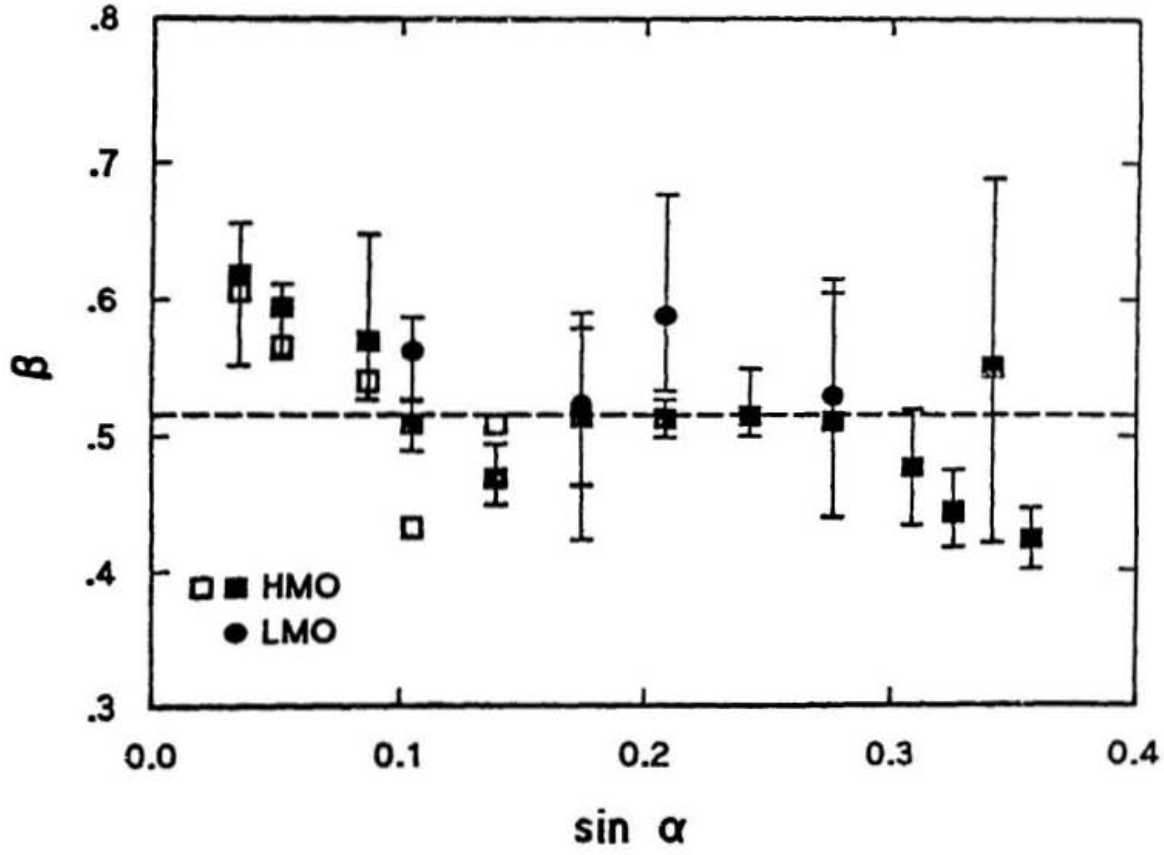

Fig. 4-3(b). Same as Fig. 4-3(a) except for HMO on plexiglass.

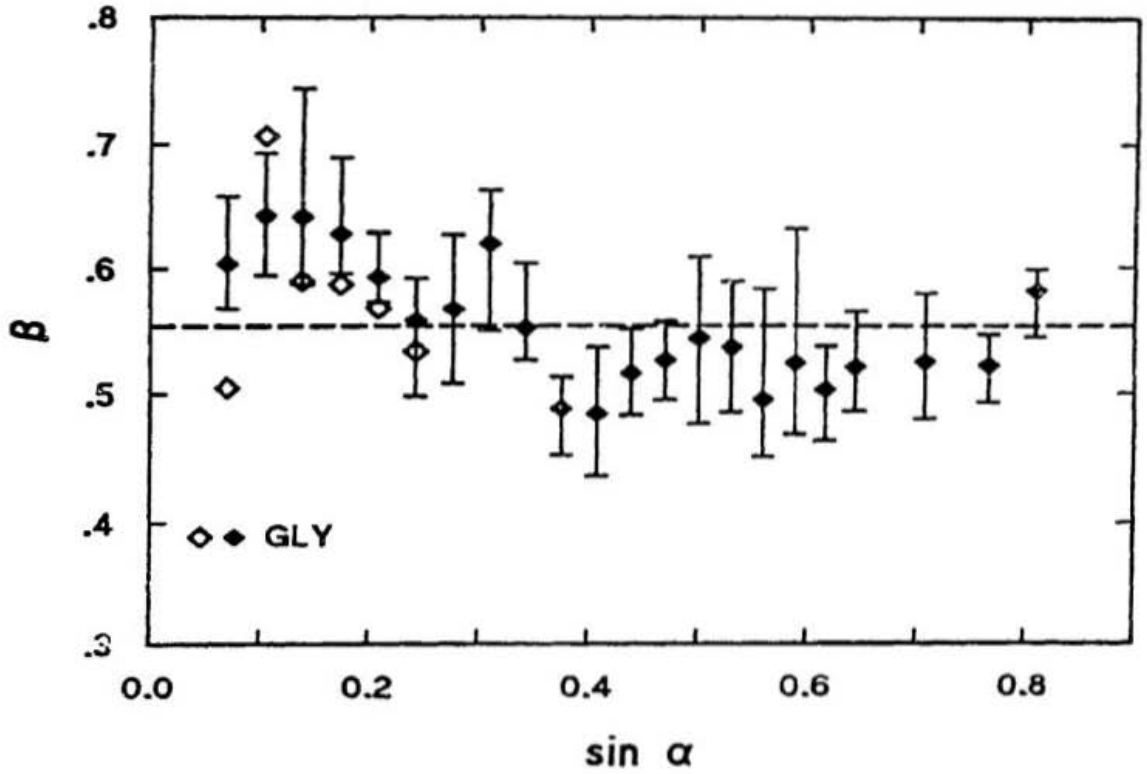

Fig. 4-3(c). Same as Fig. 4-3(a) except for glycerin on glass.

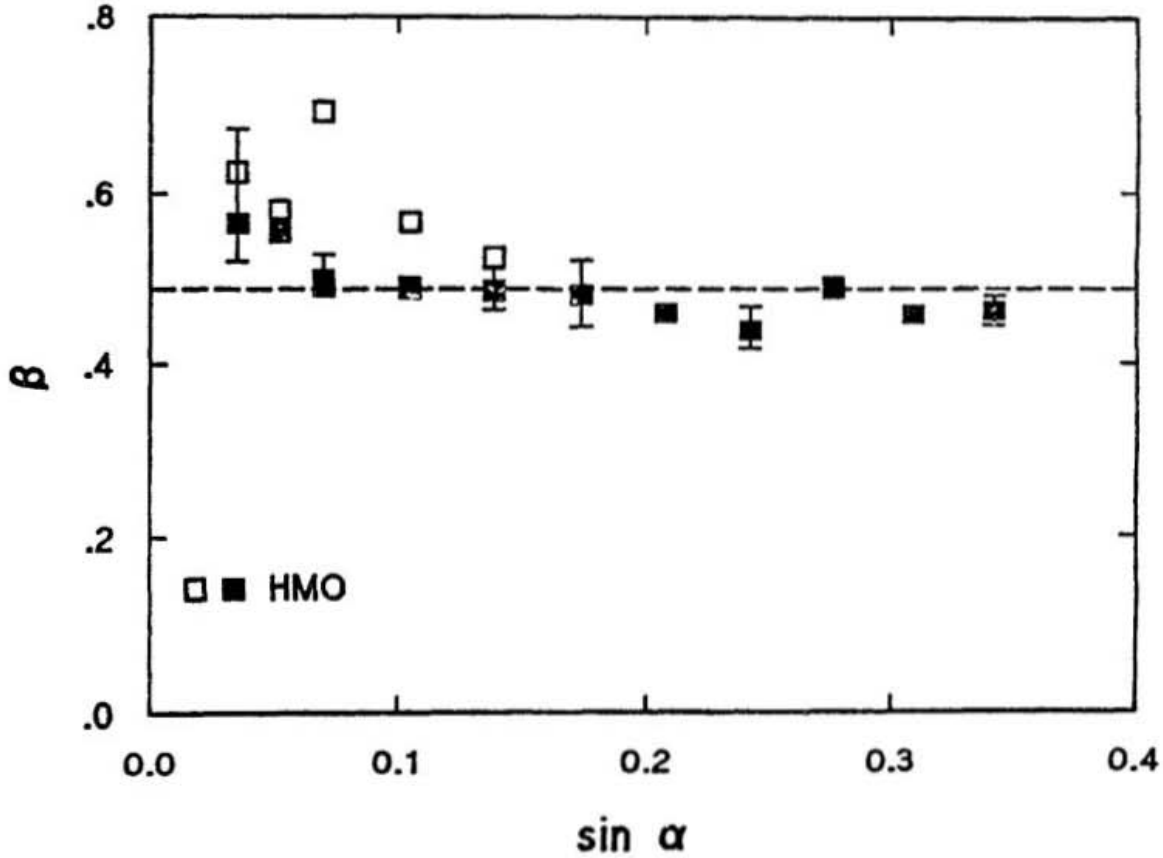

Fig. 4-3(d). Same as Fig. 4-3(a) except for HMO on glass.

(a) and (b), and glass, (c) and (d). For all fluids on both surfaces I find that

$$A = k \sin\alpha \qquad (4-4)$$

with the slope k increasing with decreasing viscosity. For the plexiglass surface, I find that $k = 11.1 \pm .5\,cm \cdot s^{-\beta}$ for glycerin, $36.4 \pm 1.6\,cm \cdot s^{-\beta}$ for HMO and $63.1 \pm 2.8\,cm \cdot s^{-\beta}$ for LMO and for the glass surface $k = 12.6 \pm .5\,cm \cdot s^{-\beta}$ for glycerin and $38.1 \pm 1.2\,cm \cdot s^{-\beta}$ for HMO. The values of A and A_0 are equal within experimental error for glycerin and HMO on both surfaces. Table II shows the values of k for glycerin and HMO on both surfaces.

In most cases the contact line position, measured at points corresponding to finger tips, varied smoothly through the instability. However in a few cases a kink appeared in the position-time plots at the onset of the instability. These are the cases for which there is a significant difference in β and β_0 apparent in Figs. 4-3 (a) to (d).

The trough positions are described by Eq. (4–3), which represents an exponential slowing of the contact line, with the trough approaching a constant downhill velocity C at large times. The exponential slowing time τ as a function of $\sin\alpha$ is shown in Figs. 4-5(a) and (b) for plexiglass and Figs. 4-5(c) and (d) for glass. For all fluids on both surfaces τ decreases with increasing α like

$$\tau = a_\tau \sin\alpha^{-b_\tau}. \qquad (4-5)$$

For the plexiglass surface $a_\tau = 3.1 \pm .4\,s$ and $b_\tau = 0.51 \pm .08$ for glycerin and $a_\tau = 0.62 \pm .19\,s$ and $b_\tau = 1.4 \pm .1$ for HMO. The glass surface gave $a_\tau = 2.7 \pm .2\,s$ and $b_\tau = 0.85 \pm .04$ for glycerin and $a_\tau = 1.9 \pm 1.0\,s$ and $b_\tau = 1.08 \pm .17$ for HMO. These results are shown in Table III.

At low angles the exponential slowing times are on the order of 1 minute for HMO on both surfaces while for glycerin it is about 15 seconds on plexiglass and 30 seconds

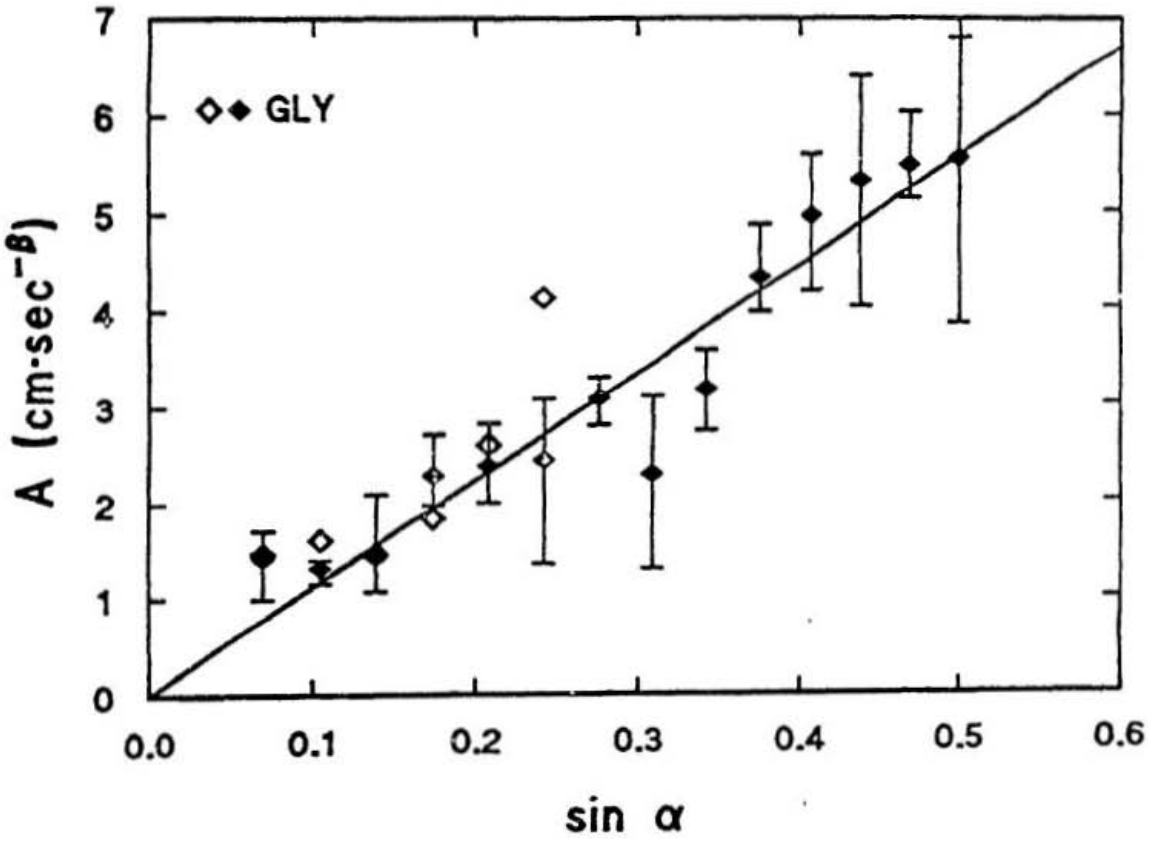

Fig. 4-4(a). The solid symbols show the amplitude A of Eq. (4–2) for glycerin on plexiglass. The lines are fits to Eq. (4–4). The open symbols show the amplitude A_0 for the flow before the instability, determined from Eq. (4–1).

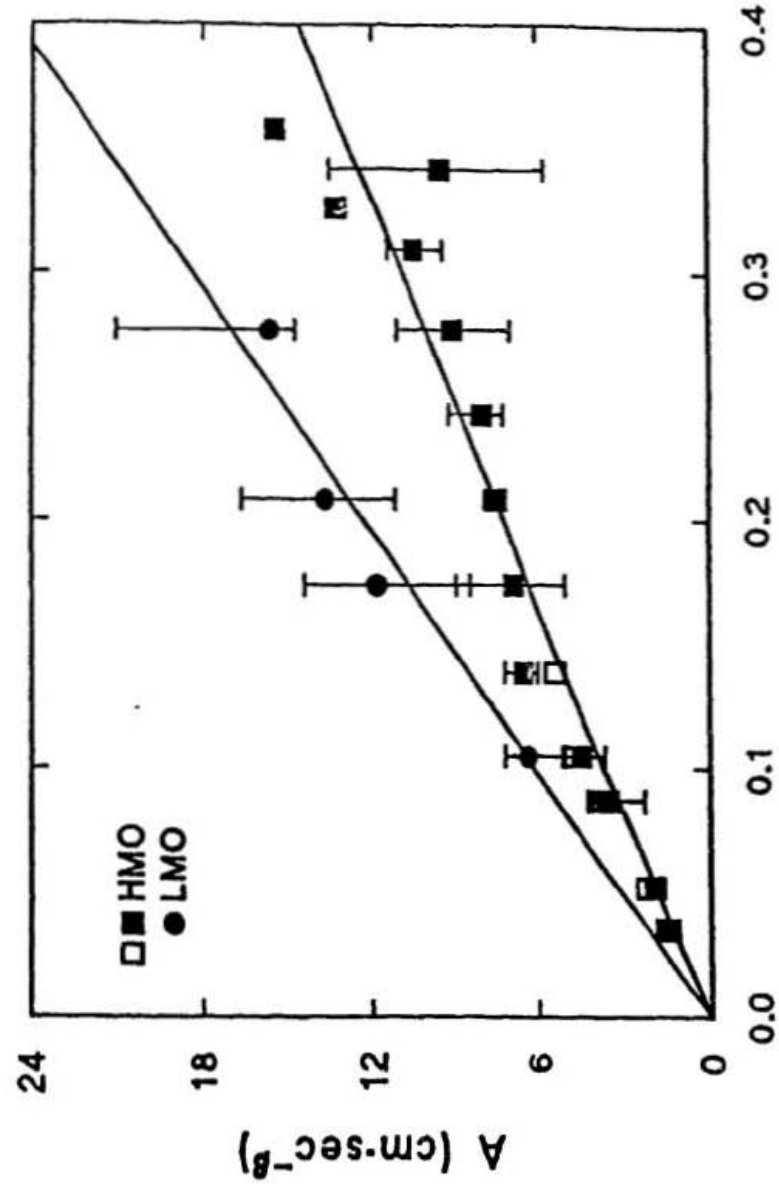

Fig. 4-4(b). Same as Fig. 4-4(a) except for HMO on plexiglass.

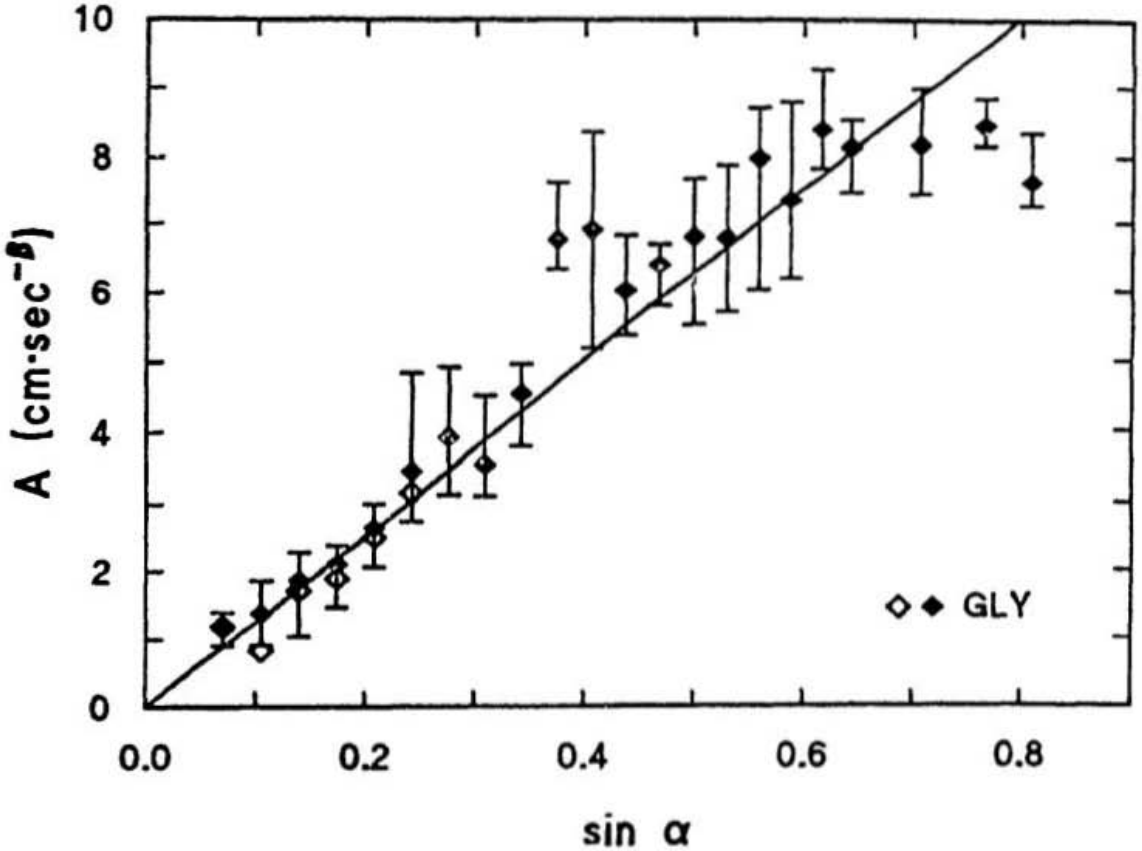

Fig. 4-4(c). Same as Fig. 4-4(a) except for glycerin on glass.

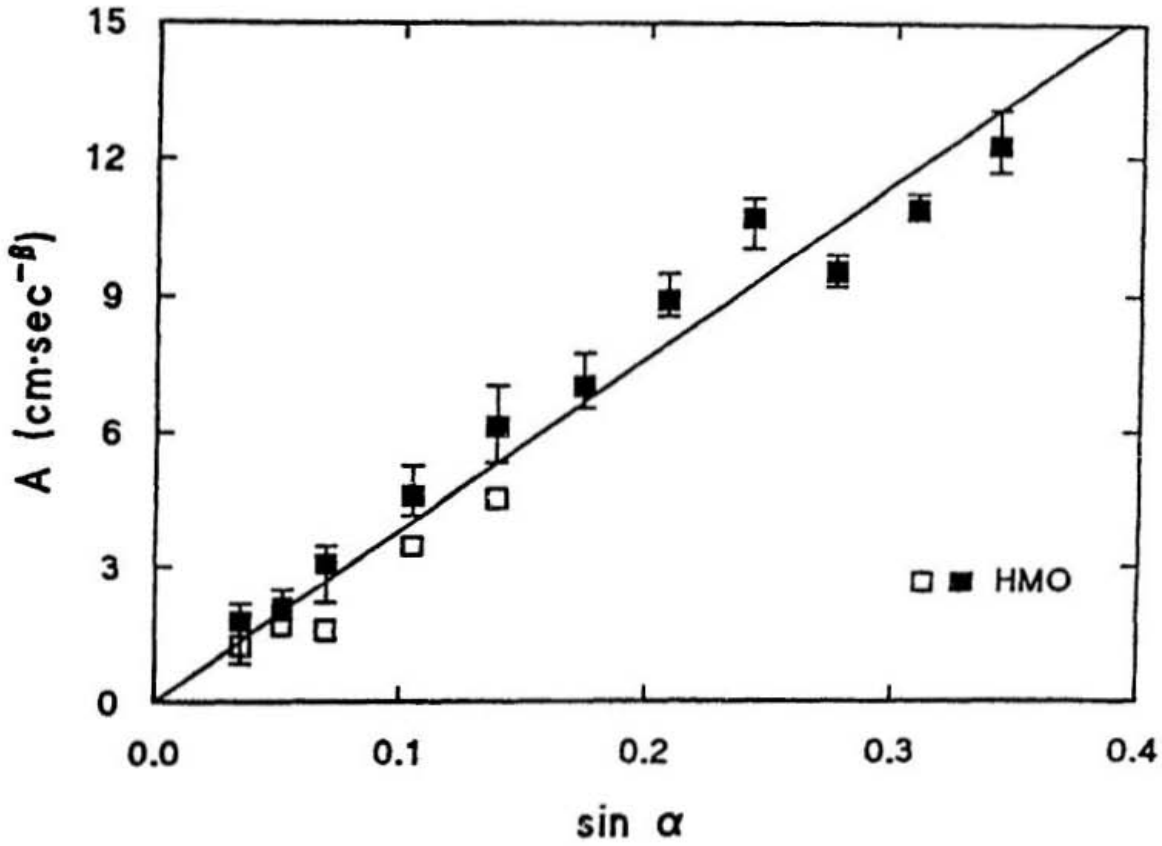

Fig. 4-4(d). Same as Fig. 4-4(a) except for HMO on glass.

Table II. Parameters characterizing the finger tip position.

	glycerin on plexiglass	glycerin on glass	HMO on plexiglass	HMO on glass
β	$0.65 \pm .04$	$0.55 \pm .05$	$0.52 \pm .05$	$0.48 \pm .01$
$k\,(cm\,s^{-\beta})$	$11.1 \pm .5$	$12.6 \pm .5$	36.4 ± 1.6	38.1 ± 1.2

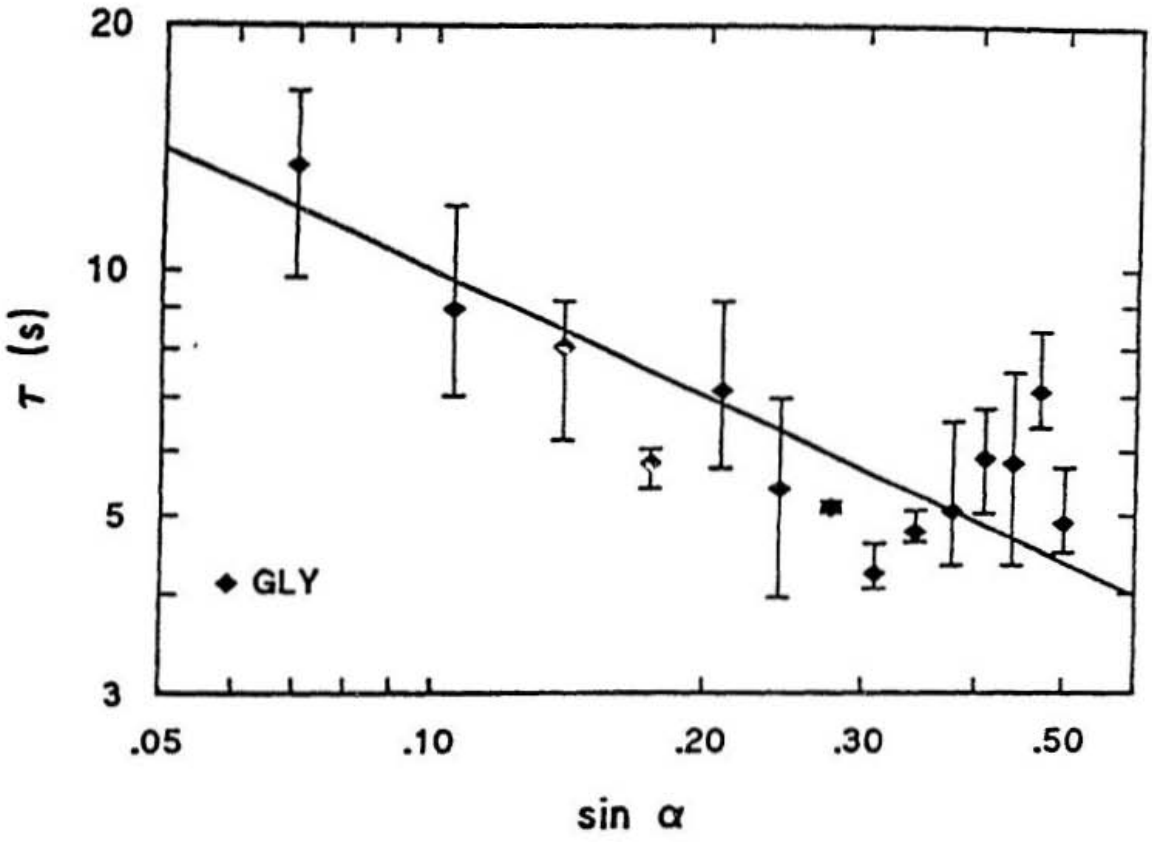

Fig. 4-5(a). The exponential slowing time τ of Eq. (4-3) as a function of $\sin\alpha$ for glycerin on plexiglass. The lines are power law fits to Eq. (4-5).

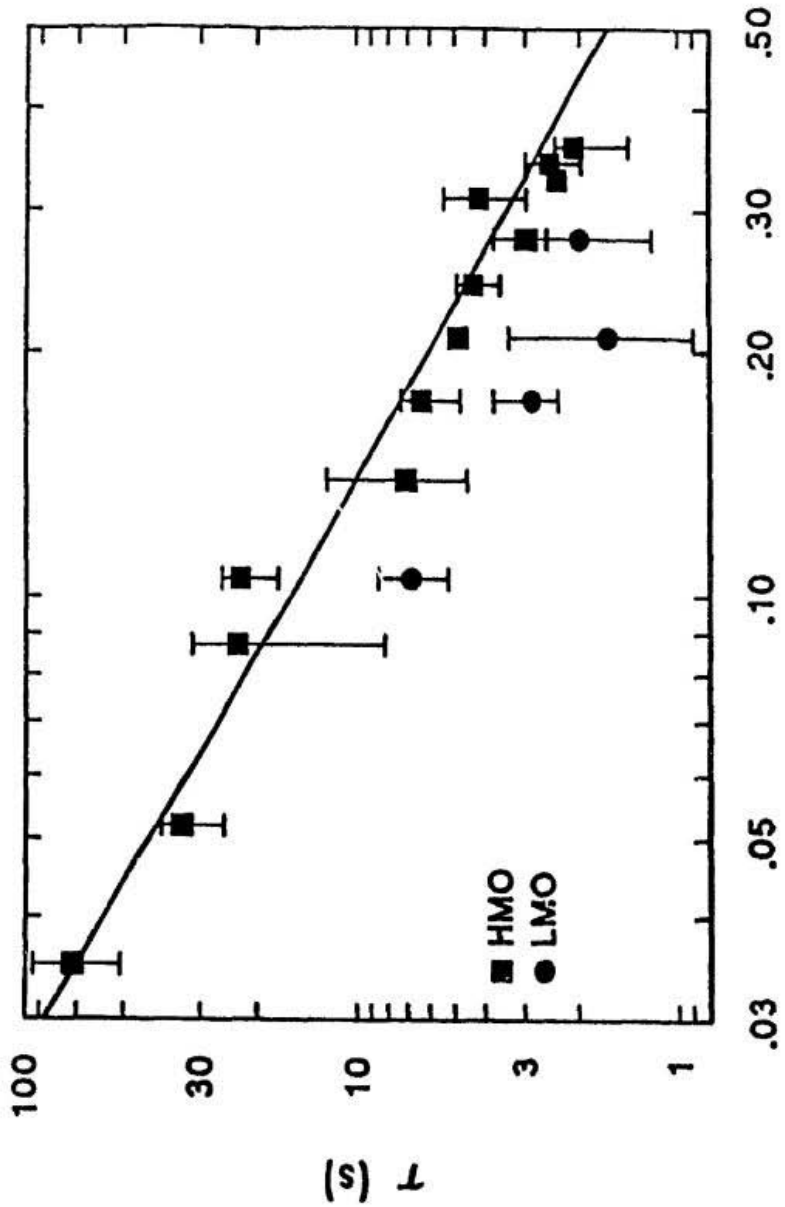

Fig. 4-5(b). Same as Fig. 4-5(a) except for HMO on plexiglass.

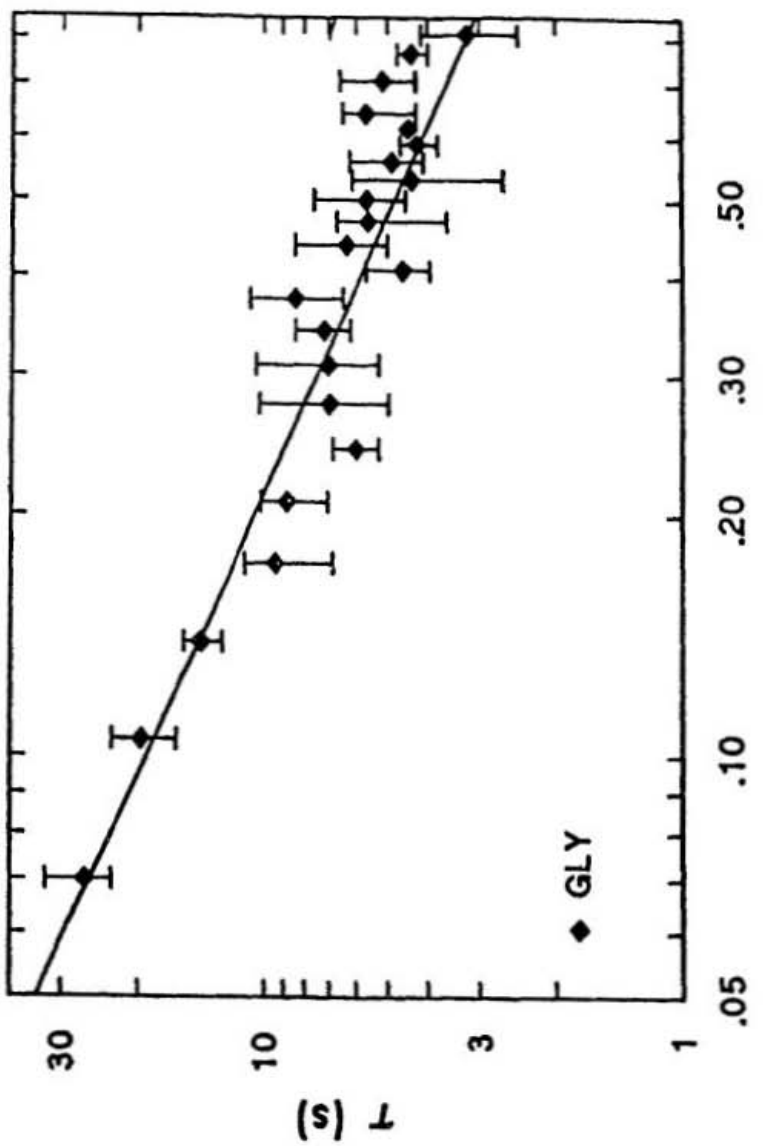

Fig. 4-5(c). Same as Fig. 4-5(a) except for glycerin on glass.

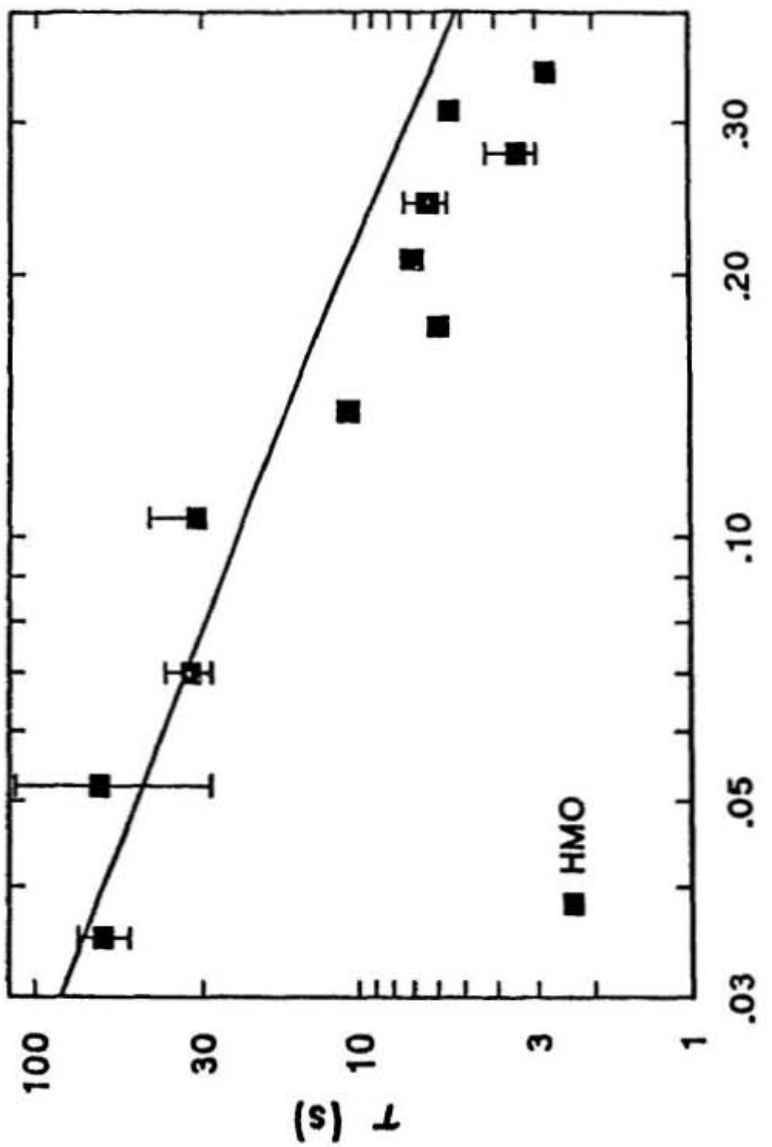

Fig. 4-5(d). Same as Fig. 4-5(a) except for HMO on glass.

on glass. However, for $\alpha \sim 17°$ the values of τ for glycerin and HMO on plexiglass are roughly equal as are the values for the two fluids on glass.

The amplitude of the exponential slowing time, B in Eq. (4-3), is shown in Figs. 4-6. B is constant within experimental scatter except at low angles. For the plexiglass surface, the average value of B at high angles, *i.e.*, not including the first two or three points, is $-10.7 \pm .9\,cm$ for glycerin and $-12.4 \pm .8\,cm$ for HMO. On glass the average value of B is $-12.9 \pm 1.0\,cm$ for glycerin and $-12.1 \pm 1.1\,cm$ for HMO. Values of B for both fluids on both surfaces are shown in Table III.

The velocity of the troughs at long times, C, is shown in Figs. 4-7(a) and (b) for plexiglass and (c) and (d) for glass. For glycerin $C = 0$ within experimental error for both surfaces at all angles studied. For HMO, however, $C \simeq 0$ at small angles, but increases smoothly and approximately linearly to about $0.1\,cm/s$ at $\alpha = 20°$ on both surfaces.

Even though the rivulet pattern which develops from the instability is not perfectly periodic, the *average* wavelength $\overline{\lambda}$ is a well defined length. $\overline{\lambda}$ is taken as the distance between two adjacent fingers averaged over the pattern, but excluding the finger at each edge which may be strongly influenced by the nearby walls. Figs. 4-8(a) and (b) show $\overline{\lambda}$ as a function of $\sin\alpha$ for plexiglass and glass respectively. Within experimental scatter the data for the different fluids on the plexiglass surface are indistinguishable. The same is true for the data for the glass surface except at low angles, where the HMO data appears to be lower than that for glycerin. $\overline{\lambda}$ for both fluids on both substrates shows a power law dependence on $\sin\alpha$:

$$\overline{\lambda} = a_\lambda \sin\alpha^{-b_\lambda}. \qquad (4-6)$$

Fits to the data for the plexiglass surface result in $a_\lambda = 2.7 \pm .2\,cm$ and $b_\lambda = 0.41 \pm .03$

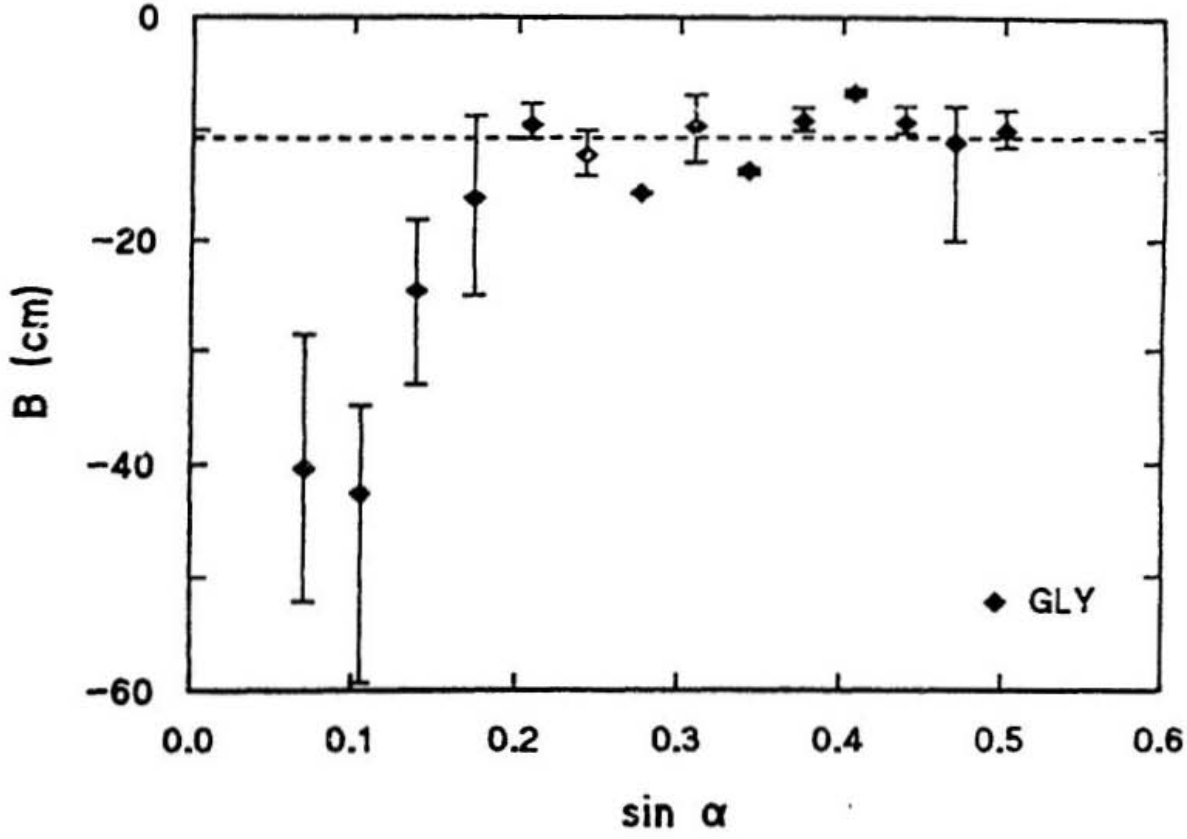

Fig. 4-6(a). The amplitude B of Eq. (4-3) as a function of $\sin\alpha$ for glycerin on plexiglass. The dashed lines show the average of each at high angles.

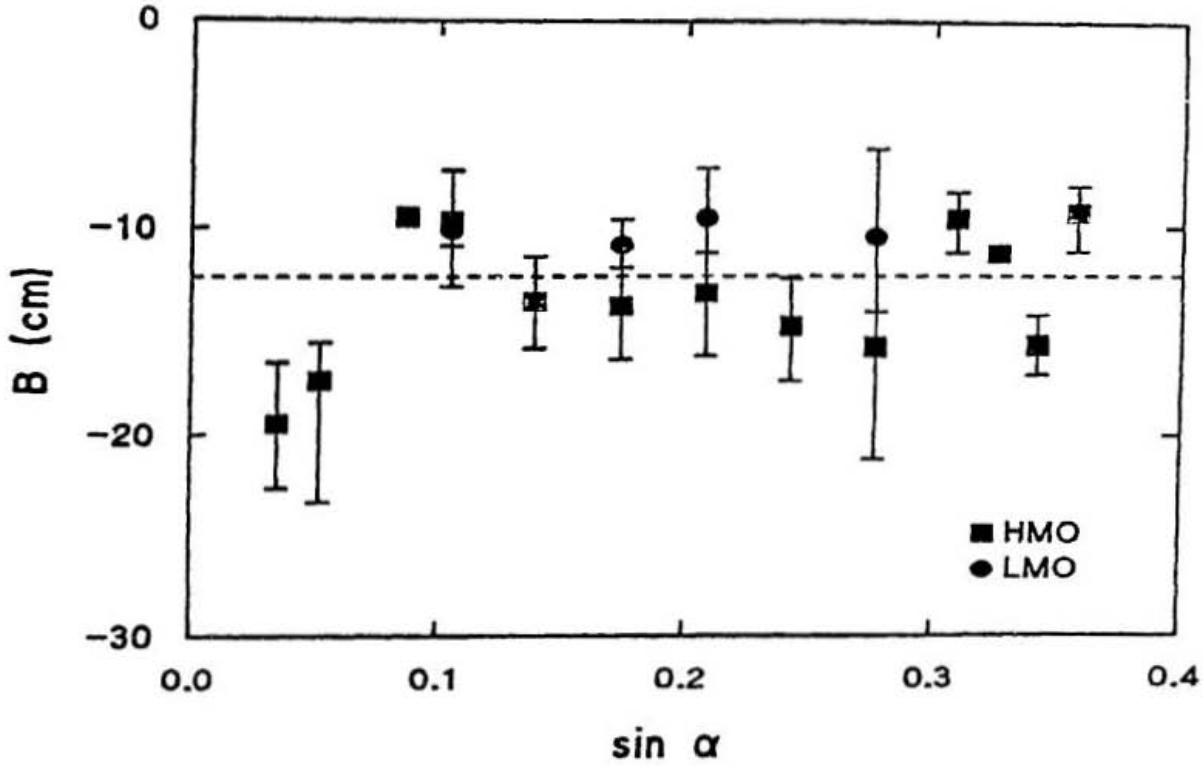

Fig. 4-6(b). Same as Fig. 4-6(a) except for HMO on plexiglass.

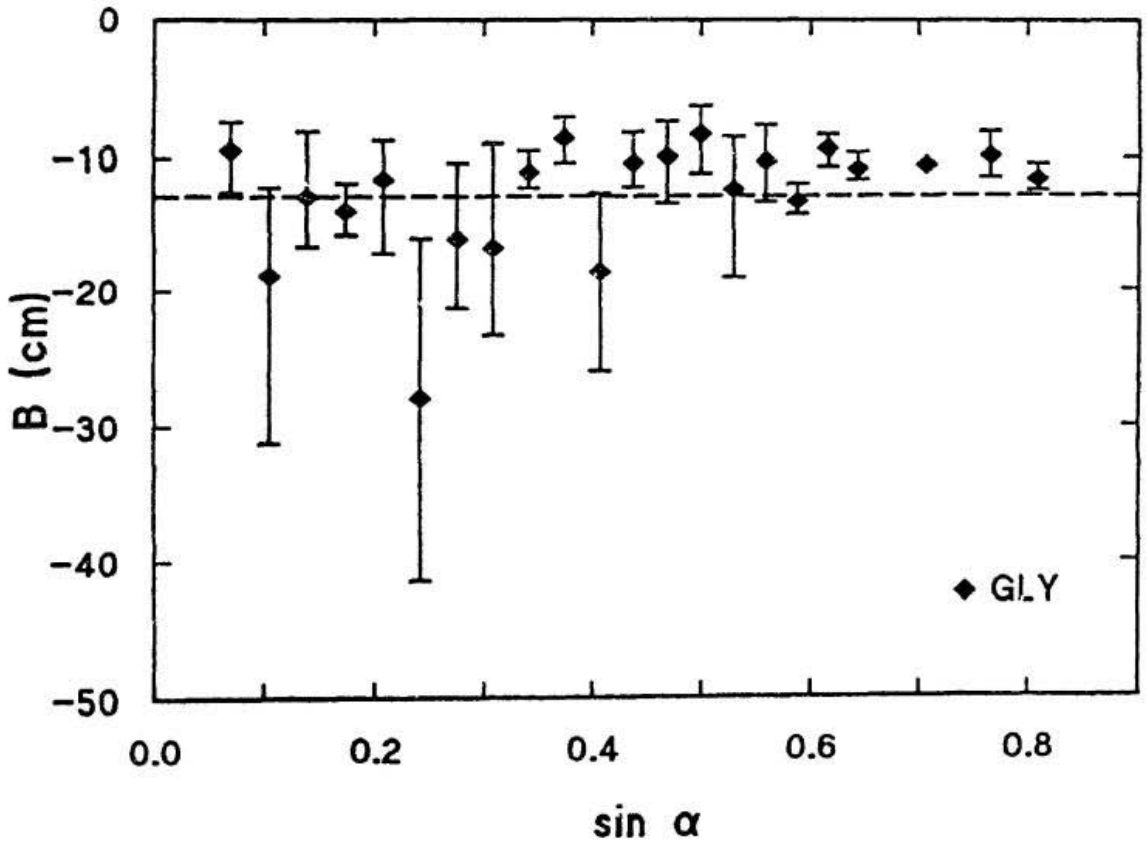

Fig. 4-6(c). Same as Fig. 4-6(a) except for glycerin on glass.

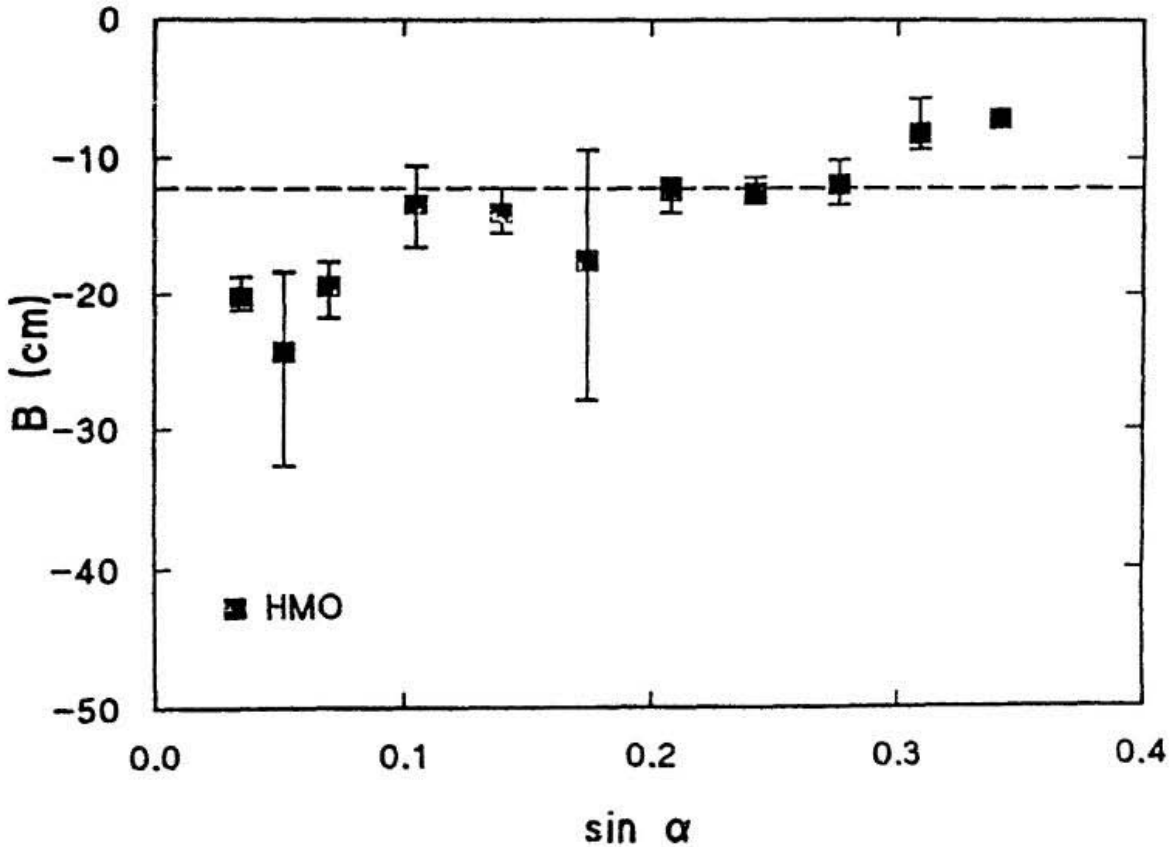

Fig. 4-6(d). Same as Fig. 4-6(a) except for HMO on glass.

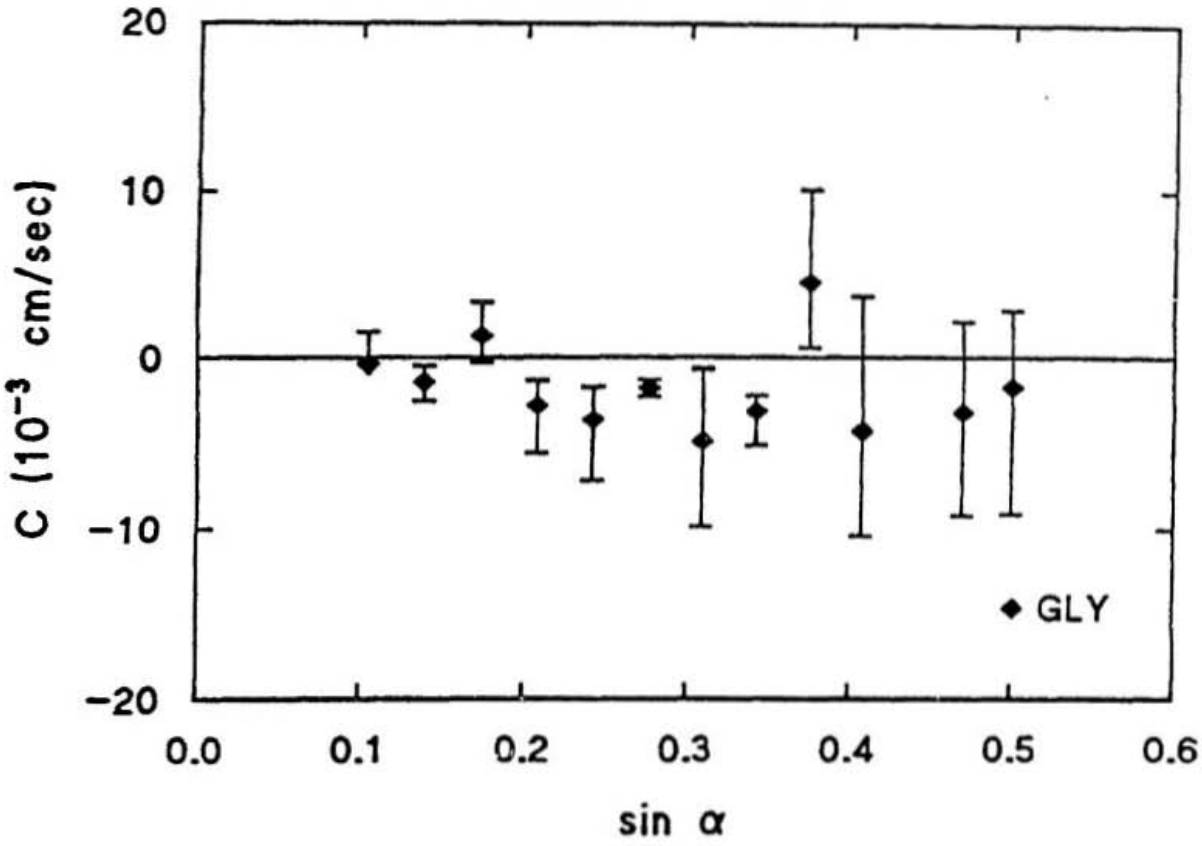

Fig. 4-7(a). The asymptotic velocity C of Eq. (4-3) as a function of $\sin\alpha$ for glycerin on plexiglass.

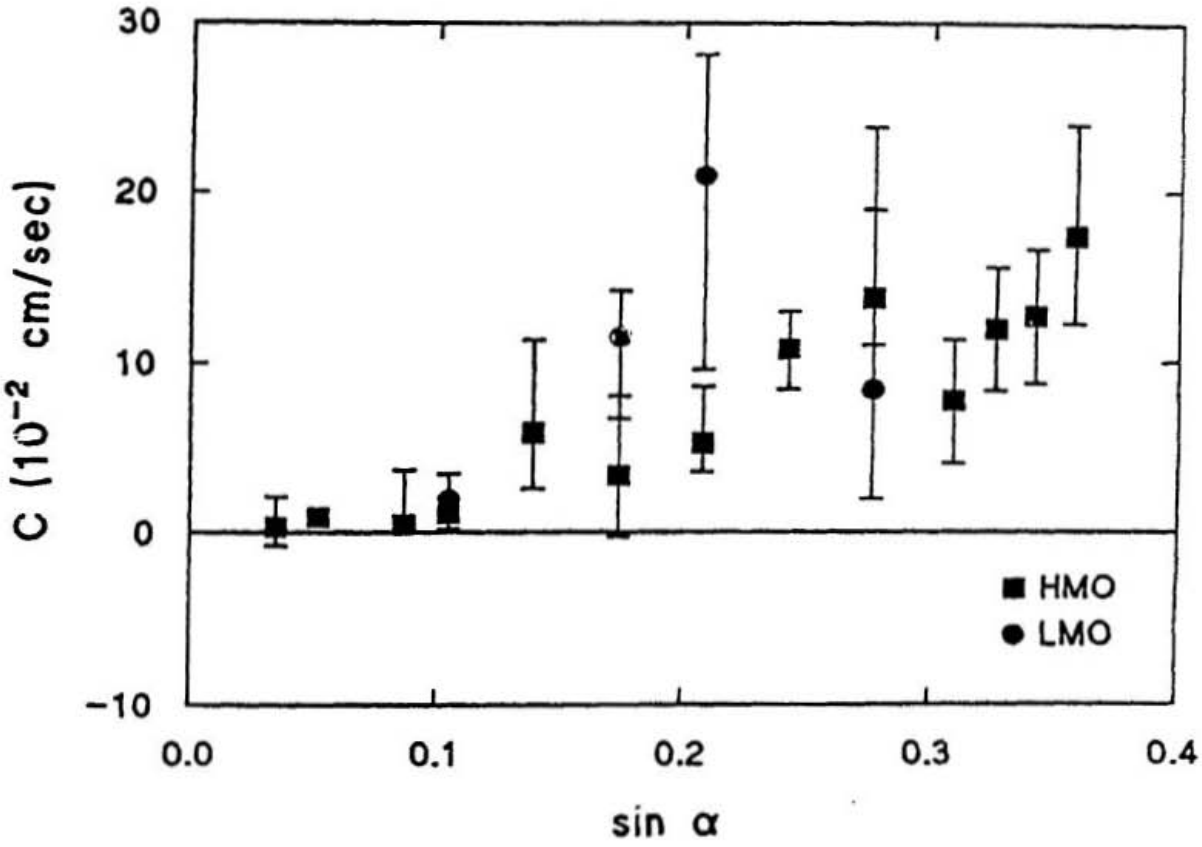

Fig. 4-7(b). Same as Fig. 4-7(a) except for HMO on plexiglass.

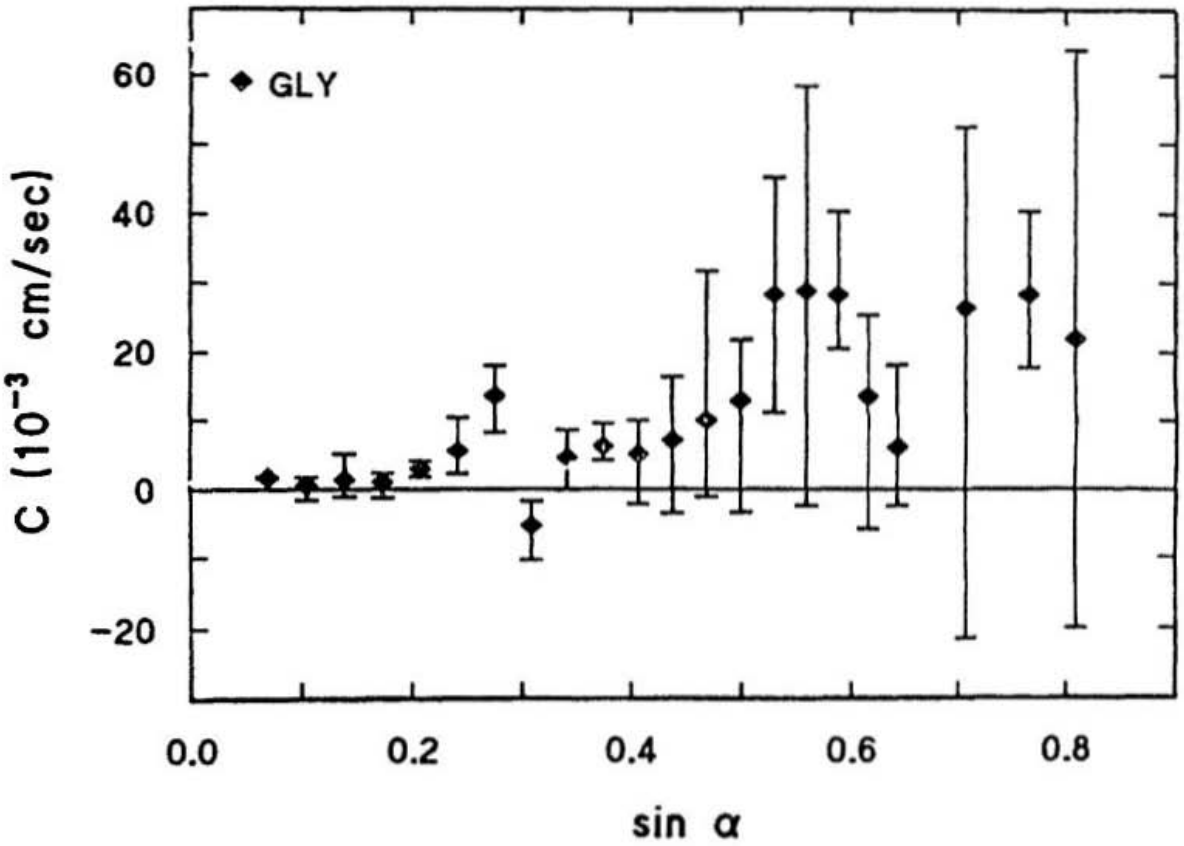

Fig. 4-7(c). Same as Fig. 4-7(a) except for glycerin on glass.

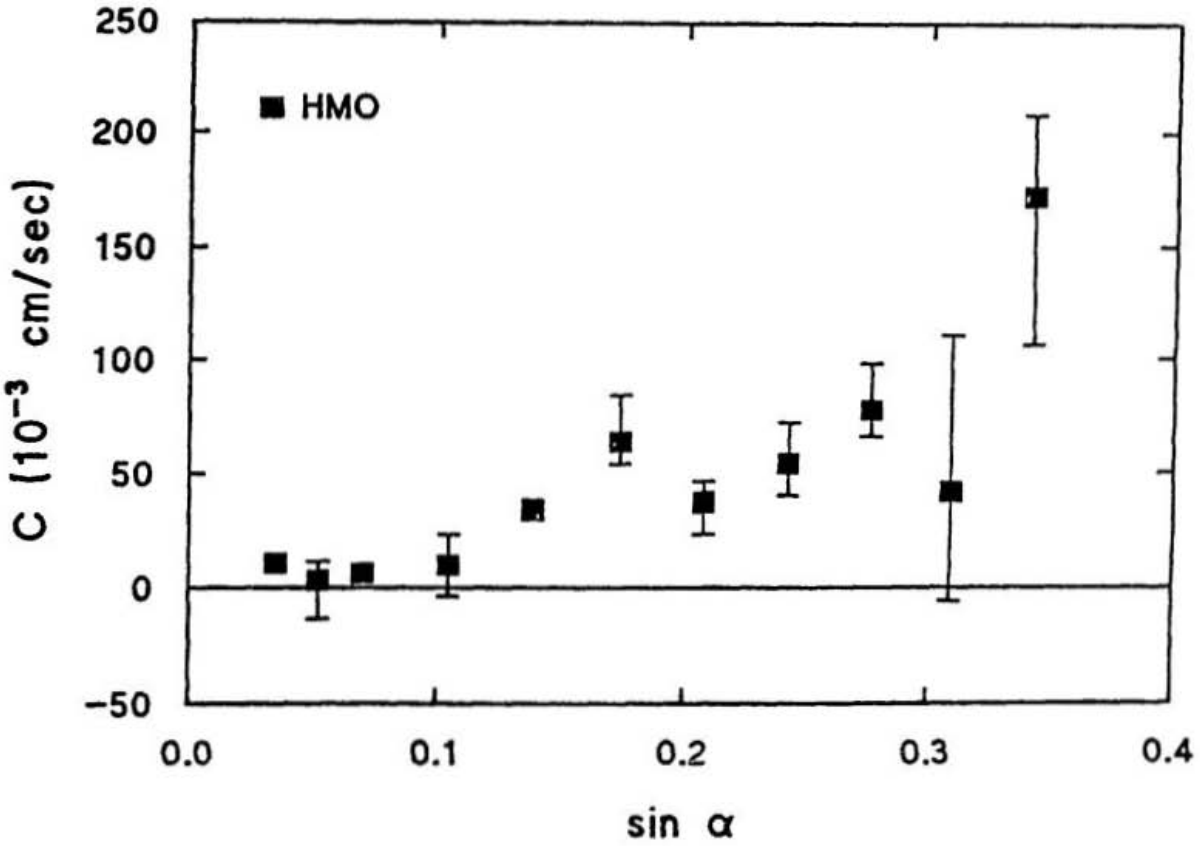

Fig. 4-7(d). Same as Fig. 4-7(a) except for HMO on glass.

Table III. Parameters characterizing the trough position.

	glycerin on plexiglass	glycerin on glass	HMO on plexiglass	HMO on glass
$a_T\,(s)$	$3.1 \pm .4$	$2.7 \pm .2$	$0.62 \pm .19$	$1.93 \pm .97$
b_T	$0.51 \pm .08$	$0.85 \pm .04$	$1.4 \pm .1$	$1.08 \pm .17$
$B\,(cm)$	$-10.7 \pm .9$	-12.9 ± 1.0	$-12.4 \pm .8$	-12.1 ± 1.1

for glycerin and $a_\lambda = 2.8 \pm .2\,cm$ and $b_\lambda = 0.40 \pm .02$ for HMO. The fits for the glass surface give $a_\lambda = 2.5 \pm .1\,cm$ and $b_\lambda = 0.49 \pm .02$ for glycerin and $a_\lambda = 3.0 \pm .4\,cm$ and $b_\lambda = 0.39 \pm .05$ for HMO. Performing fits to each of these data sets using the 1/3 exponent predicted by Huppert[1] yields for the plexiglass surface $a_\lambda{}^* = 3.03 \pm .07\,cm$ for glycerin and $a_\lambda{}^* = 3.23 \pm .08\,cm$ for HMO and for the glass surface $a_\lambda{}^* = 3.11 \pm .09\,cm$ for glycerin and $a_\lambda{}^* = 3.38 \pm .13\,cm$ for HMO. These values for a_λ, b_λ and $a_\lambda{}^*$ are shown in Table IV.

The widths of individual fingers are very uniform across the pattern and vary only slightly along the length of a given finger. I found that this width, measured half way along the length of a finger, also varies as a power law in $\sin\alpha$:

$$\delta = a_\delta \sin\alpha^{-b_\delta}, \qquad (4-7)$$

as shown in Fig. 4-9(a) for plexiglass and Fig. 4-9(b) for glass. Fits to the data for the plexiglass surface yield $a_\delta = 0.68 \pm .04\,cm$ and $b_\delta = 0.53 \pm .03$ for glycerin and $a_\delta = 0.86 \pm .10\,cm$ and $b_\delta = 0.66 \pm .04$ for HMO, while for the glass surface $a_\delta = 0.91 \pm .05\,cm$ and $b_\delta = 0.51 \pm .03$ for glycerin and $a_\delta = 0.98 \pm .05\,cm$ and $b_\delta = 0.59 \pm .04$ for HMO. These values of a_δ and b_δ are shown in Table IV. For comparison I also show a line of $-1/3$ slope in Figs. 4-9(a) and (b); such a slope is not consistent with my data.

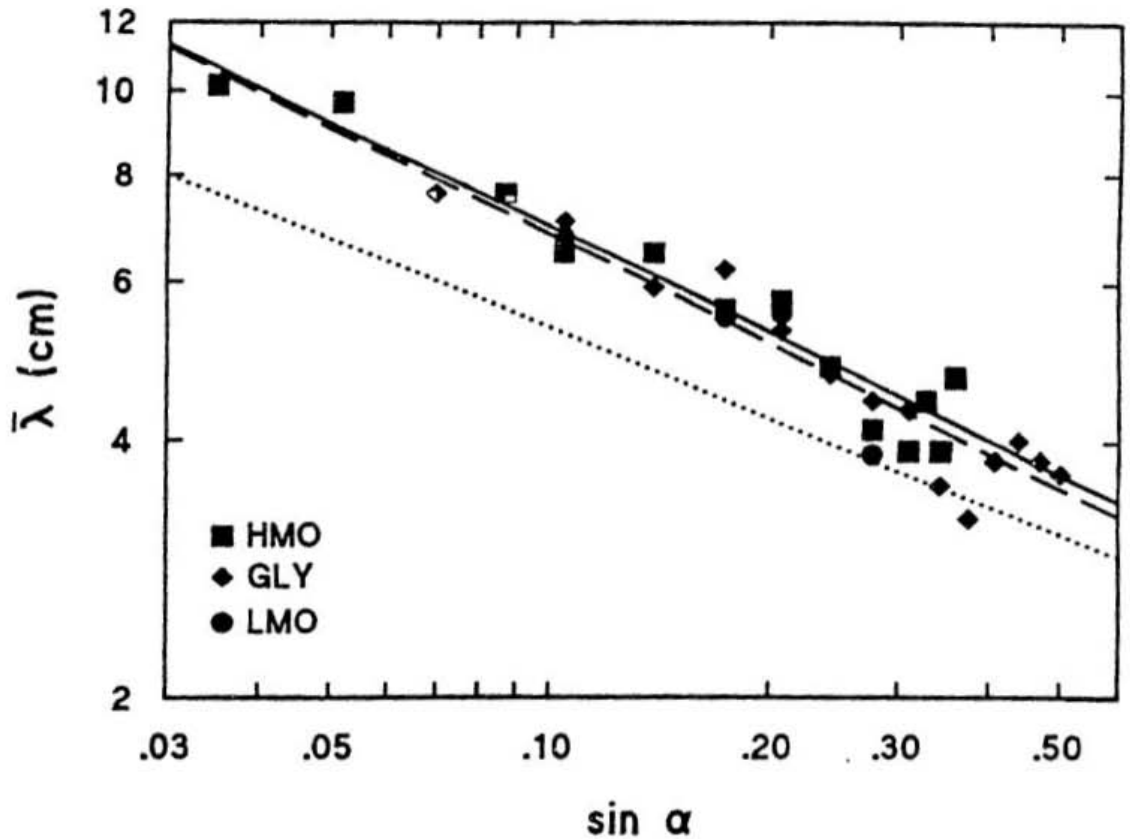

Fig. 4-8(a). The average wavelength $\bar{\lambda}$ of the finger patterns for the plexiglass surface. ——— is a fit of Eq. (4–6) to data for HMO with $b_\lambda = 0.40 \pm .02$. — — — is a similiar fit for glycerin with $b_\lambda = 0.41 \pm .03$ and ····· is a line of slope $-1/3$ for comparison.

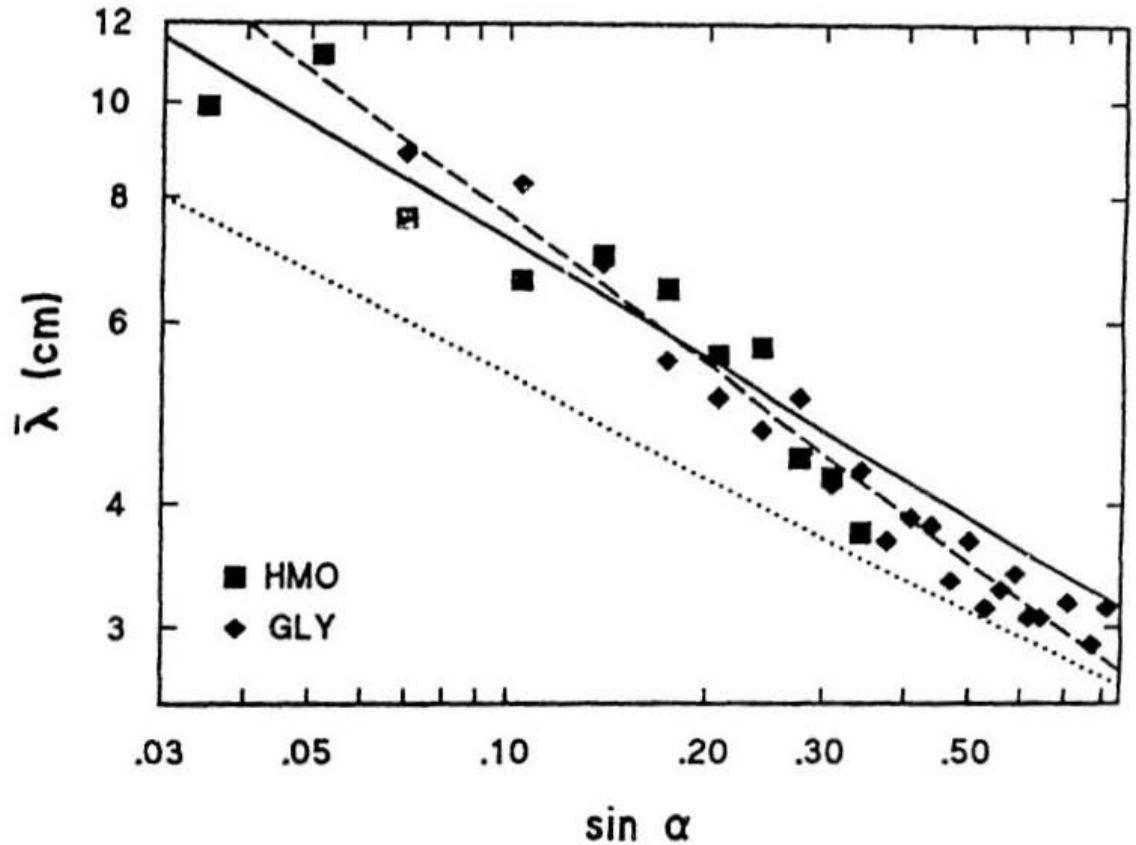

Fig. 4-8(b). Same as Fig. 4-8(a) except for the glass surface with $b_\lambda = 0.39 \pm .05$ for HMO and $b_\lambda = 0.49 \pm .02$ for glycerin.

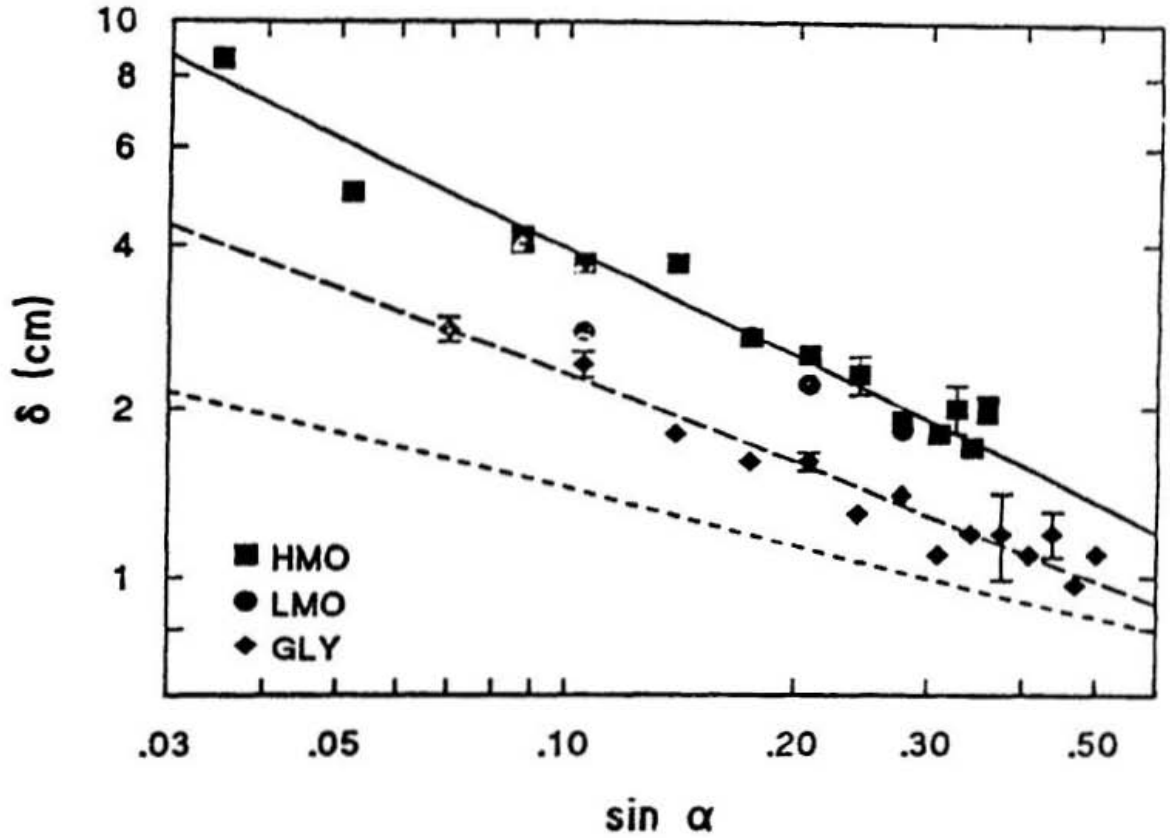

Fig. 4-9(a). The finger width δ as a function of $\sin\alpha$ for the plexiglass surface. ——— is a fit of Eq. (4-7) to data for HMO with $b_\zeta = 0.66 \pm .04$. — — — is a similiar fit for glycerin with $b_\delta = 0.53 \pm .03$.

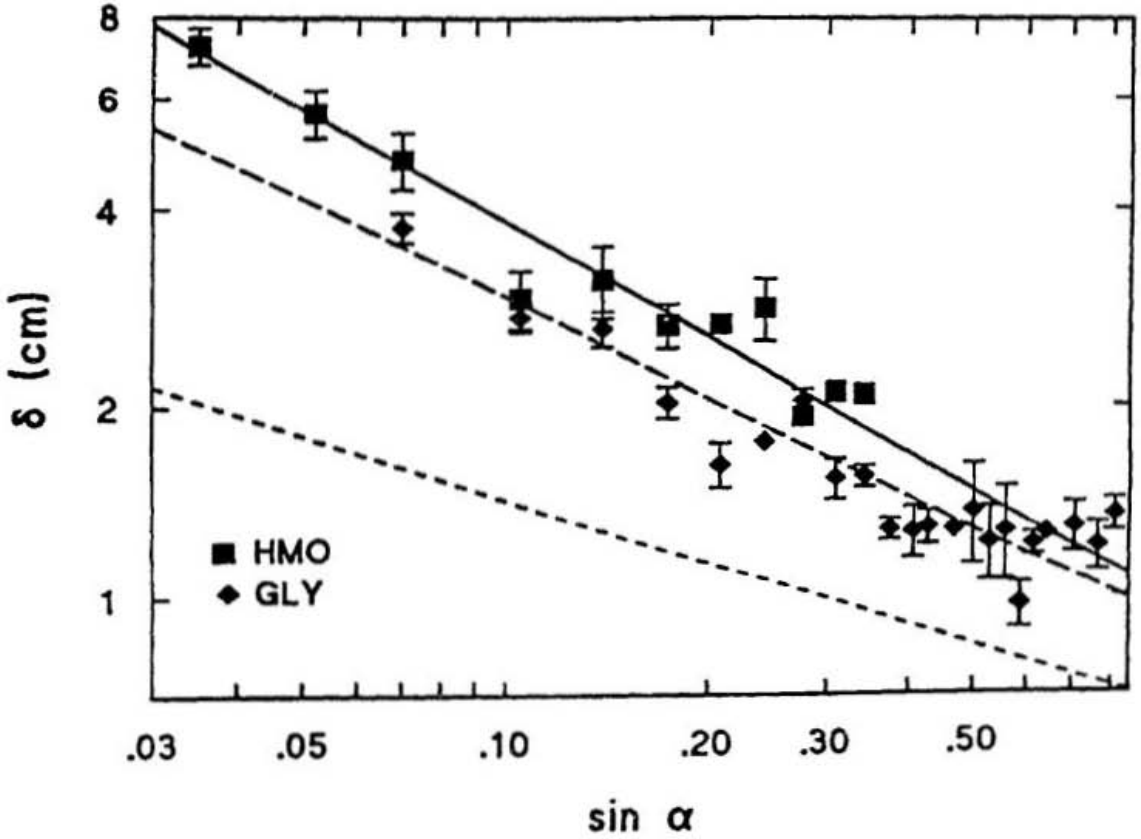

Fig. 4-9(b). Same as Fig. 4-9(a) except for the glass surface with $b_\delta = 0.59 \pm .04$ for HMO and $b_\delta = 0.51 \pm .03$ for glycerin.

Table IV. Parameters characterizing the wavelength and finger width.

	glycerin on plexiglass	glycerin on glass	HMO on plexiglass	HMO on glass
$a_\lambda\,(cm)$	$2.7 \pm .2$	$2.5 \pm .1$	$2.8 \pm .2$	$3.0 \pm .4$
b_λ	$0.41 \pm .03$	$0.49 \pm .02$	$0.40 \pm .02$	$0.39 \pm .05$
$a_\lambda{}^*\,(cm)$	$3.03 \pm .07$	$3.11 \pm .09$	$3.23 \pm .08$	$3.38 \pm .13$
$a_\delta\,(cm)$	$0.68 \pm .04$	$0.91 \pm .05$	$0.86 \pm .10$	$0.98 \pm .02$
b_δ	$0.53 \pm .03$	$0.51 \pm .03$	$0.66 \pm .04$	$0.59 \pm .04$

Chapter 5 Discussion

5.1 Before Instability

My results for the flow of this fluid sheet before the instability show a somewhat more complicated behaviour than that implied in Ref. (1). Huppert[1] found both experimentally and theoretically that, prior to the instability, the position of the contact line moved downhill like $x \sim t^{1/3}$. At all but the smallest angles studied, my data are also consistent with a power law behaviour, but with an exponent larger than 1/3. Within the experimental error, the exponents I determined for the flow before and after the instability are the same - about 1/2 for HMO and about 2/3 for glycerin on both surfaces. However, at the smallest angles for both fluids my results, shown in Fig. 4-1, indicate that the flow approaches $t^{1/3}$ growth at long times while at earlier times it advances with an exponent larger than 1/3. Thus the approximate equality of the exponents before and after the instability may be coincidental.

Huppert[1] studied this flow in the lubrication approximation, neglecting surface tension. In section 2.7 I followed his procedure and derived an equation for the shape of the free surface $h(x,t)$

$$\frac{\partial h}{\partial t} + (g \sin \alpha/\mu) h^2 \frac{\partial h}{\partial x} = 0 \qquad (5-1)$$

and using this derived an equation for the position of the uniform contact line,

$$x_n = (9A^2 g \sin \alpha/4\mu)^{1/3} t^{1/3}. \qquad (5-2)$$

Flow governed by Eq. (5–1) will evolve into a shock, and x_n is the position of the shock. Eq. (5–2) is valid when $x_n \gg l$, and at long times when the initial conditions no longer significantly affect the flow. In my experiments the first condition is always

true — $x_n/l \sim 15$ for glycerin at small α and is larger for larger angles and for HMO — but my data indicate that the second condition is almost never true, *i.e.*, the initial conditions affect the flow of the uniform contact line right up to the time at which the instability develops. Further experiments with more viscous fluids — to increase the time before the instability — are necessary to study this behaviour in more detail.

5.2 After Instability

Both Huppert[1] and Silvi and Dussan V[2] observed experimentally, as did I, that the glycerin on plexiglass resulted in the rivulet pattern developing. However, for glycerin on glass they observed the sawtooth pattern while I observed the rivulet pattern. This may be due to the condition of the surfaces. Since neither Huppert nor Silvi and Dussan V give any description of the cleaning procedure used, the condition of the surfaces may have been different, *i.e.*, my surface or their surfaces may have had a slight film after cleaning due to the procedure and/or cleaning agent(s) used.

I can also compare my results with previous work on the behaviour of the average wavelength, $\overline{\lambda}$. From my experiments $\overline{\lambda}$ is observed to have a power law dependence on $\sin\alpha$ but not with the exponent of 1/3 predicted by Eq. (1-2); the experimental exponents, shown in Table V, are consistent, except for glycerin on glass. Huppert also predicted, Eq. (1-2), that $\overline{\lambda}$ should vary with fluid properties like $(\sigma/\rho)^{1/3}$. From my fits of $\overline{\lambda}$ to Eq. (4-6) with the exponent fixed at 1/3 gives $\overline{\lambda}_{HMO}/\overline{\lambda}_{GLY} = 1.07 \pm .04$ for plexiglass and $1.09 \pm .07$ for glass, while $(\sigma_{HMO}\,\rho_{GLY}/\sigma_{GLY}\,\rho_{HMO})^{1/3} = 0.94 \pm .04$. Thus I observe no significant difference in $\overline{\lambda}$ between the two fluids on either substrate. However the predicted difference is small.

From fits to Eq. (4-6) with $b_\lambda = 1/3$ I determined the constant of proportionality in Eq. (1-2) for the plexiglass surface to be $7.0 \pm .4$ for glycerin and $8.0 \pm .3$ for HMO,

while the glass surface gives $7.2 \pm .3$ for glycerin and $8.3 \pm .4$ for HMO. These are consistent with the results of Refs. (1) and (2) which quote 7.5 and 8, respectively.

The finger width δ did not display the same α-dependence as did $\overline{\lambda}$, and while $\overline{\lambda}$ is approximately the same for the fluids on both surfaces, δ is not. This points to $\overline{\lambda}$ and δ being governed by different physical mechanisms. While the length scale of the instability, *i.e.*, $\overline{\lambda}$, depends on the competition between gravitational and surface tension forces at the contact line,[1,12] δ will be a function of the properties of the fluid. The finger must have a certain cross-sectional area in order to accomodate the fluid which is flowing down it. Thus the width of the finger will depend on the static liquid-solid contact angle. If the contact angle along the side of the finger is larger (smaller) than the maximum (minimum) static value, then the finger will become wider (narrower) until the contact angle decreases (increases) to its maximum (minimum) static value, but the cross-sectional area of the finger will remain constant.

I discuss the work of Troian *et al.*[13] in chapter 2 where they apply linear stability analysis to the equations for a film flowing under the influence of gravity. Their theoretical analysis differs from my experiments in two repects. The first is that a precursor film does not appear to exist in my experiments, and the second is that the analysis of Ref. (13) is valid only in the limit $3Ca \ll \tan\alpha^{1/3}$, *i.e.*, for large angles, while for my experiments $3Ca/\tan\alpha^{1/3} \sim 3$. Although the experimental situation is somewhat different from the theoretical one, it is interesting to compare my results with the predictions of Ref. (13).

Troian *et al.*[13] study the stability of the calculated profile by imposing periodic perturbations on the contact line and studying the growth of these perturbations. They find that the profile is unstable for wavenumbers $q \lesssim .9$ with a maximum

growth rate for $\lambda = 14l$ where $l = h/(3\,Ca)^{1/3}$ is a characteristic length.

I can calculate the ratio $\overline{\lambda}/l$ for my data by first estimating the film thickness at the contact line to be

$$h = 3A/2x_n, \qquad (5-3)$$

from Huppert's[1] expression, Eq. (2-19), where x_n is the length of the flow at the onset of the instability. I find $h \approx 0.33\,cm$ for glycerin and $h \approx 0.27\,cm$ for HMO on both substrates. The velocity U is estimated from results of fits to Eq. (4-2), along with the observation, discussed above, that the flow velocity varies smoothly through the instability. Then

$$U = dx_d/dt = \beta A(t - t_0)^{\beta-1}, \qquad (5-4)$$

evaluated at the point of instability. Also from above we have

$$A = k\sin\alpha \qquad (5-5)$$

and from fits to Eq. (4-6) with $b_\lambda = 1/3$,

$$\overline{\lambda} = a_\lambda{}^* \sin\alpha^{-1/3}. \qquad (5-6)$$

Thus

$$\overline{\lambda}/l = \frac{a_\lambda{}^*}{h}\left(\frac{3\mu\beta k}{\sigma}\right)^{1/3}(t - t_0)^{(\beta-1)/3}. \qquad (5-7)$$

From my measurements I find that $(t - t_0)$ is a function of $\sin\alpha$ and the data for plexiglass are reasonably well described by

$$\begin{aligned} t - t_0 &= 1.9\sin\alpha^{-1.0} \qquad \text{(glycerin)} \\ &= 0.53\sin\alpha^{-1.3}, \qquad \text{(HMO)} \end{aligned} \qquad (5-8a)$$

while for glass

$$\begin{aligned} t - t_0 &= 1.9\sin\alpha^{-0.9} \qquad \text{(glycerin)} \\ &= 2.0\sin\alpha^{-0.9}. \qquad \text{(HMO)} \end{aligned} \qquad (5-8b)$$

Using my results for the relevent parameters and the fluid properties from Table I, I find for plexiglass

$$\begin{aligned} \overline{\lambda}/l &= 14.1 \sin\alpha^{0.12} \qquad \text{(glycerin)} \\ &= 19.2 \sin\alpha^{0.21}, \qquad \text{(HMO)} \end{aligned} \tag{5-9a}$$

while for glass

$$\begin{aligned} \overline{\lambda}/l &= 13.6 \sin\alpha^{0.12} \qquad \text{(glycerin)} \\ &= 12.4 \sin\alpha^{0.16}. \qquad \text{(HMO)} \end{aligned} \tag{5-9b}$$

I estimate the accumulated uncertainties in the coefficients of Eqs. (5-9a) and (5-9b) to be on the order of 20%. This percentage is estimated after taking into account the standard errors in $a_\lambda{}^*$, β and k, the uncertainties in the experimentally determined physical properties σ and μ and the uncertainty in estimating the film thickness h. These functions are plotted in Figs. 5-1(a) and 5-1(b) for the plexiglass and glass surfaces, respectively, along with the prediction of Troian *et al.*[13]

The experiments performed here are confined to $\alpha < 22°$ for HMO on both surfaces, $\alpha < 32°$ for glycerin on plexiglass and $\alpha < 55°$ for glycerin on glass, while the theory is valid for large angles ($3\,Ca \ll \tan\alpha^{1/3}$); despite this the agreement between their prediction and the extrapolation of my results to large angles is quite reasonable.

In my experiments the advancing front was never perfectly periodic. A possible explanation comes from the results of Troian *et al.* who find that the contact line is unstable for a range of wavenumbers $q \lesssim 0.9$, Fig. 2-6, with a maximum growth rate for $\lambda = 14l$. A superposition of several high growth rate wavelengths may contribute to the imperfect periodicity of the pattern which develops.

My results for the various fitting parameters can be categorized in terms of their dependence on the physical properties of the system studied. I found that $\overline{\lambda}$ was essentially independent of fluid and surface for fluids and surfaces I studied, depending

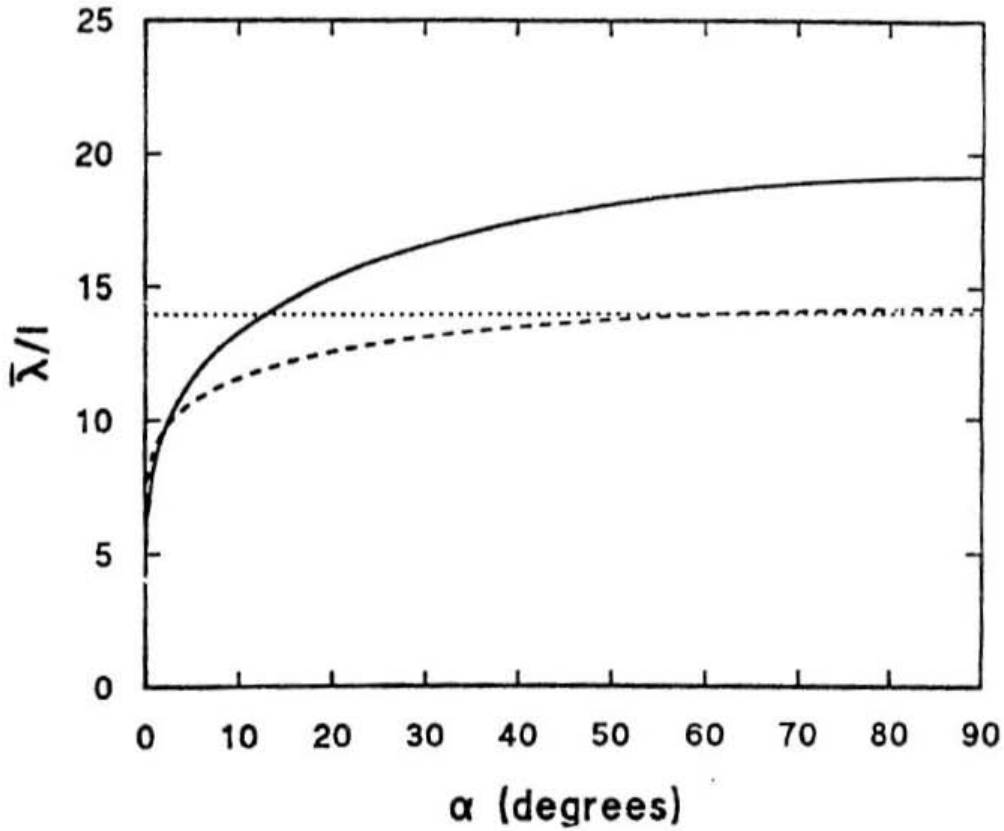

Fig. 5-1(a). The ratio $\bar{\lambda}/l$ from my experimental results for the plexiglass surface along with the theoretical prediction of reference 12. ——— HMO; — — — glycerin; ····· theoretical result.

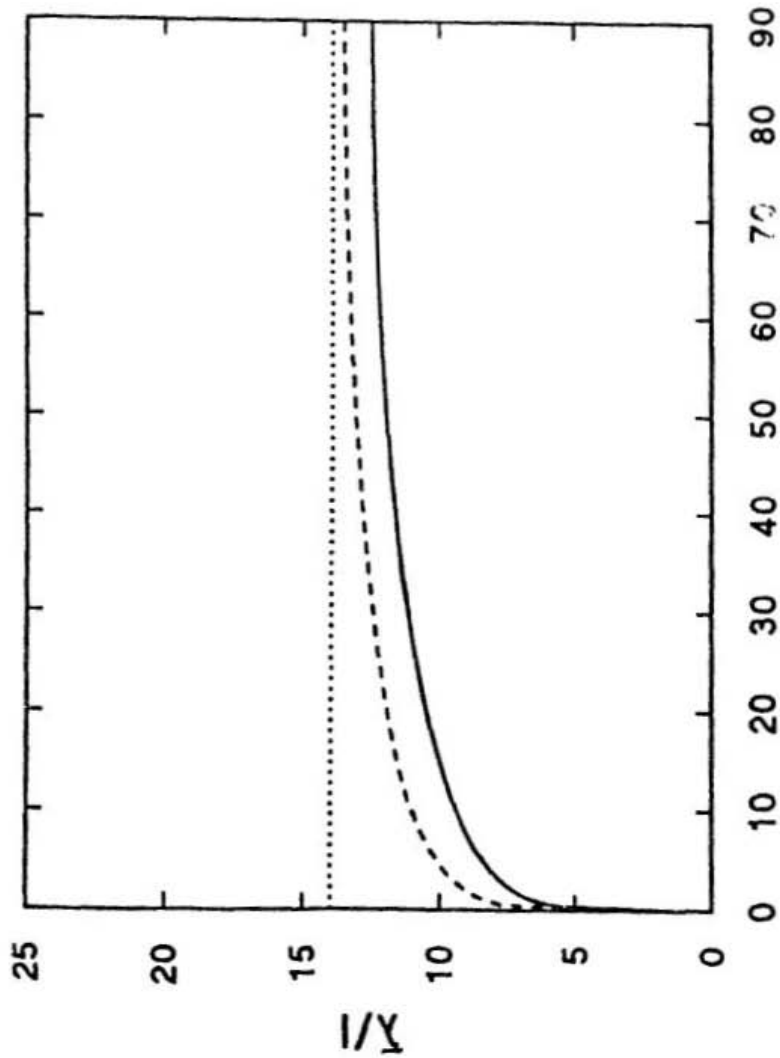

Fig. 5-1(b). Same as Fig. 5-1(a) except for the glass surface.

only on the slope angle α. The weak dependence on fluid properties predicted by Huppert[1] was not observed, although more study of this point is needed. The finger width δ was indistinguishable for HMO on both surfaces while δ for glycerin on glass was slightly larger than for the plexiglass surface. The finger width of HMO was larger than that for glycerin for both surfaces. This may be due to glycerin's larger static contact angle, which allows a narrow glycerin finger to have the same cross-sectional area as a wider HMO finger.

The fitting parameter A — the amplitude in the finger growth expression, Eq. (4-2) — increased with decreasing viscosity and seemed independent of surface for the surfaces studied here. All other fitting parameters — the growth exponent β of the rivulets, and the slowing time τ, amplitude B, and asymptotic velocity C of the troughs — are equal within experimental error for the two oils, and thus apparently independent of viscosity. At higher angles, $\alpha \gtrsim 8°$, the amplitude B of the exponential slowing term in Eq. (4-3) is constant and equal within experimental uncertainties for all fluids on both surfaces. The differences between the values of the other parameters for glycerin and HMO for each surface probably reflects a dependence on the surface tension or, as Silvi and Dussan V[2] point out, on the liquid-solid contact angle.

I used the fitting functions Eqs. (4-2) and (4-3) simply because they gave a good description of my data, although the use of Eq. (4-2) was motivated partially by the results of Huppert.[1] The physical significance of these fitting parameters is not clear and a more complete theoretical treatment of the problem is required before they can be considered as anything other than empirical.

Finally I will consider the evolution of the fingers, and following Silvi and Dussan V[2] I will think in terms of the local contact angle $\theta(y)$ at the liquid-solid-air contact

line. For a typical liquid-solid system the contact angle is a function of the speed of the moving contact line having the general form of Fig. 2-2. For contact angles $\theta_R \leq \theta \leq \theta_A$ the contact line does not move, for $\theta > \theta_A$ it advances in the direction perpendicular to its local tangent, and for $\theta < \theta_R$ it recedes. A straight contact line, advancing with uniform velocity v_1, will have $\theta(y) = \theta_1$, say, with $\theta_1 > \theta_A$, as illustrated in Fig. 5-2.

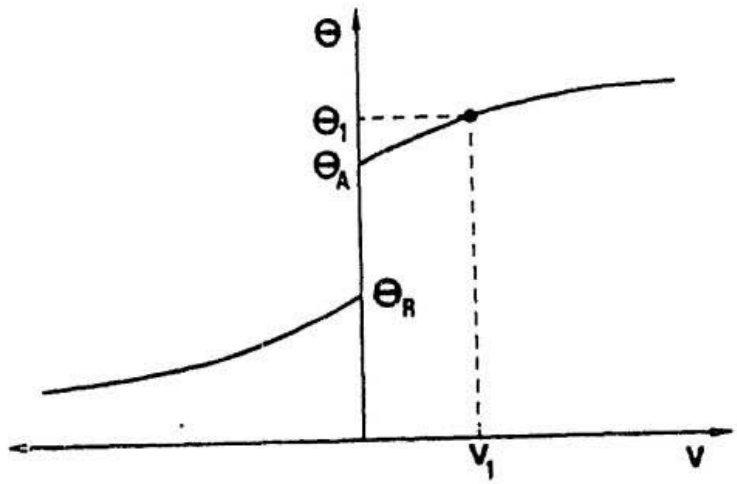

Fig. 5-2. The general form of the contact angle θ at the liquid-solid-vapor contact line, as a function of contact line velocity. Here it is shown that some advancing contact angle θ_1 is advancing with velocity v_1.

As the straight contact line becomes unstable, the contact angle will begin to vary with y. Faster-moving regions of the front will have $\theta(y) > \theta_1$ while slower moving regions will have $\theta_A < \theta(y) < \theta_1$. If the contact angle at some point drops below θ_A, that point will stop. Thus for the rivulet pattern, $\theta(y) < \theta_A$ in the trough region while $\theta(y) > \theta_A$ near the tips.

Consider the situation sketched in Fig. 5-3, where the solid line represents the contact line shortly after the onset of the instability.

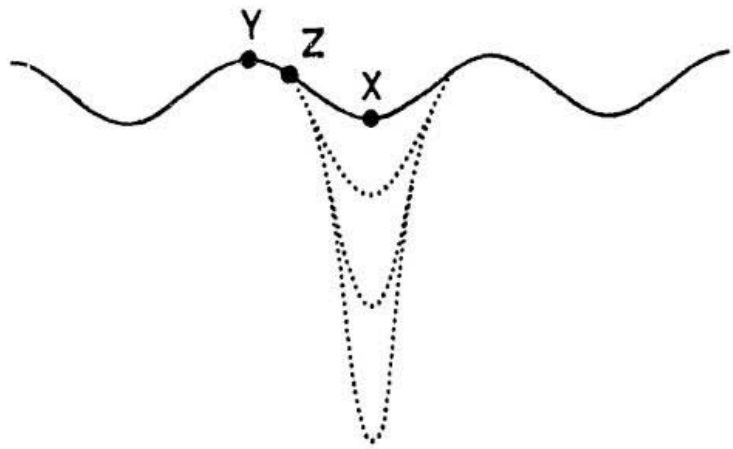

Fig. 5-3. The contact line shortly after the onset of the instability is sketched as a solid line. θ is greater than, less than and equal to θ_A at the points X, Y and Z respectively. The dotted lines show schematically the growth of a rivulet.

Clearly $\theta(X) > \theta_A$ at the point X at the tip of the developing finger. Assume that $\theta(Y) < \theta_A$ at Y, in the trough. Then there is a point Z at which $\theta(Z) = \theta_A$; at points downslope from Z the contact line will advance perpendicular to its local tangent. Because of the relation between contact angle and the speed of advance of the contact line, as the finger develops its sides will become more and more oriented in the downslope direction. This reduces the gravitational pressure along the sides, and so reduces θ there. Thus the point at which $\theta = \theta_A$ moves downslope, eventually settling near the tip of the finger. As sketched in Fig. 5-3 this process leads to fingers with straight sides oriented downslope, exactly as observed experimentally.

As Silvi and Dussan V point out, the sawtooth pattern will result if $\theta(y) > \theta_A$ everywhere on the contact line; θ must be smaller in the more slowly advancing troughs than at the tips.

Figs. 4-7 show the asymptotic velocity C of the troughs. For glycerin $C = 0$ within experimental error at all inclination angles indicating that $\theta(y)$ is indeed less than θ_A in the trough regions. However, for HMO C is small but nonzero at larger angles, indicating that $\theta(y) \gtrsim \theta_A$ in the trough regions for angles $\alpha \gtrsim 8°$. This result suggests that the sawtooth pattern should form at higher angles for HMO because $\theta(y) > \theta_A$ everywhere on the contact line, but the rivulet pattern is actually observed. The explanation for this lies in the relative downslope speeds of the fingers and troughs. The finger speed is so much greater than that of the troughs that the fingers grow much faster, resulting in the rivulet pattern. Hocking[10] suggests that the sawtooth pattern is only a transitory phenomenon which will eventually evolve into the rivulet pattern if the surface is long enough. There may not actually be a sharp division between the sawtooth and rivulet patterns, but rather a continuous range of patterns with these as the two extremes. The silicone oil on glass produces a good example of the sawtooth pattern while glycerin on glass produces a good example of the rivulet pattern. HMO on glass and plexiglass produces a pattern somewhere between a perfect sawtooth and perfect rivulet pattern but leaning more toward the rivulet.

Silvi and Dussan V state that the *size* of the contact angle is the important parameter in determining which of the two patterns will evolve for a given system.[2] On the basis of the above discussion, it seems that the *shape* of the $\theta(v)$ curve is also important. If θ is a relatively flat function of v, a small decrease in θ will cause a large reduction in the contact line velocity and may even cause it to stop. On

the other hand, if θ varies steeply with v, a small decrease in θ will cause only a small decrease in the contact line velocity and most probably will not cause it to stop, and the sawtooth pattern will occur. The presence or absence of contact angle hysteresis, discussed in section 2.3, would also be expected to affect the observed pattern. Detailed measurements of contact angles along the front would be useful in confirming this picture.

Chapter 6 Conclusions

6.1 Conclusions

In this thesis I have attempted to characterize the behaviour of a viscous fluid flowing down an inclined plane, and, in particular, the pattern of fingers that develop from the contact line instability. Except at the smallest angles, the uniform contact line became unstable before the flow had relaxed to the expected $t^{1/3}$ growth. For the fluids studied here, the growth of the fingers after the instability is well described by a power law in time, while the troughs show an exponential slowing to a final velocity equal, or close to, zero. The average wavelength of the pattern decreases with increasing inclination angle, while the width of the fingers decreases more steeply with increasing α. The exponent b_λ for glycerin on glass was found to be $0.49 \pm .02$ from fits to Eq. (4-6), but looking at Fig. 4-8(b) it appears higher but not inconsistent with $-1/3$. Furthermore, fits to Eq. (4-6) with $b_\lambda = 1/3$ result in a coefficient for glycerin on glass of $a_\lambda{}^* = 3.03 \pm .07$ similar to other fits as shown in Table IV. My analysis was based primarily on fits of Eqs. (4-2) and (4-3) to measurements of the contact line position. The fit results are summarized in Table V. A theoretical treatment of this problem is required to make clear the physical meaning of the fit parameters and to explain their dependence on fluid properties, slope angle and experimental surface.

6.2 Future Considerations

There are several open questions concerning the contact line instability that warrent further study. Some measurements which could be done in the future using this apparatus are suggested in this section.

One important point concerns the behaviour of the film before the instability. In order to study the advance of the stable contact line, and to determine if it eventually

does advance like $t^{1/3}$, a fluid much more viscous than glycerin could be used at relatively small inclination angles. The larger viscosity should slow the fluid motion, making a detailed study of the flow possible.

Measurement of the film thickness, before the instability, near the front as a function of time may give a clearer picture of how the film thickness affects the contact line stability. Also measurement of the flow profile before and after the instability would be interesting, as would be the measurement of the contact angle as a function of position along the front.

Fluids which completely wet the surface, *e.g.* silicone oils, could be used to study the sawtooth pattern. Some experiments with one silicone oil ($\mu = 0.5\, g/cm\, s$, $\sigma = 20\, dyne/cm$, $\rho = .963\, g/cm^3$ and $\theta \simeq 0°$) suggest that the sawtooth pattern develops when the fluid completely wets the surface. More detailed experiments are needed to confirm this, and to characterize the sawtooth pattern flow.

Fluids of differing viscosities but similar static contact angles and surface tensions could be used to study the effect, if any, of viscosity on the instability development. Experiments to study this are now being performed using glycerin diluted with water. The water decreases the viscosity and static contact angle of the glycerin while not greatly affecting its surface tension. Studies which varied other fluid properties independently would also be interesting, *e.g.* the σ/ρ dependence of λ could be checked.

Table V. Summary of data from Tables II, III and IV.

	glycerin plexiglass	glycerin glass	HMO plexiglass	HMO glass
β	$0.65 \pm .04$	$0.55 \pm .05$	$0.52 \pm .05$	$0.48 \pm .01$
$k\,(cm\,s^{-\beta})$	$11.1 \pm .5$	$12.6 \pm .5$	36.4 ± 1.6	38.1 ± 1.2
$a_\tau\,(s)$	$3.1 \pm .4$	$2.7 \pm .2$	$0.62 \pm .19$	$1.93 \pm .97$
b_τ	$0.51 \pm .08$	$0.85 \pm .04$	$1.4 \pm .1$	$1.08 \pm .17$
$B\,(cm)$	$-10.7 \pm .9$	-12.9 ± 1.0	$-12.4 \pm .8$	-12.1 ± 1.1
$a_\lambda\,(cm)$	$2.7 \pm .2$	$2.5 \pm .1$	$2.8 \pm .2$	$3.0 \pm .4$
b_λ	$0.41 \pm .03$	$0.49 \pm .02$	$0.40 \pm .02$	$0.39 \pm .05$
$a_\lambda{}^*\,(cm)$	$3.03 \pm .07$	$3.11 \pm .09$	$3.23 \pm .08$	$3.38 \pm .13$
$a_\delta\,(cm)$	$0.68 \pm .04$	$0.91 \pm .05$	$0.86 \pm .10$	$0.98 \pm .02$
b_δ	$0.53 \pm .03$	$0.51 \pm .03$	$0.66 \pm .04$	$0.59 \pm .04$

References

1. H.E. Huppert, *Nature* **300**, 427 (1982).

2. N. Silvi and E.B. Dussan V., *Phys. Fluids* **28**, 5 (1985).

3. F. Melo, J.F. Joanny, and S. Fauve, *Phys. Rev. Lett.* **63**, 1959 (1989).

4. For a review see P.G. Gennes, *Rev. Mod. Phys.* **57**, 827 (1985).

5. E.B. Dussan V., *Ann. Rev. Fluid Mech.* **11**, 371 (1979).

6. T. Young, *Philos. Trans. R. Soc. London* **95**, 65 (1805).

7. O. Reynolds, *Philos. Trans. R. Soc. London, Ser. A* **117**, 157 (1886).

8. Lord Rayleigh, *Philos. Mag.* **30**, 285 (1890).

9. L.W. Schwartz, *Phys. Fluids A* **1**, 443 (1989).

10. L.M. Hocking, *J. Fluid Mech.* **211**, 373 (1990).

11. L.H. Tanner, *La Recherche* **17**, 182 (1986).

12. R. Goodwin and G.M. Homsy, *Phys. Fluids A* **3**, 515 (1991).

13. S.M. Troian, E. Herbolzheimer, S.A. Safran, and J.F. Joanny, *Europhys. Lett.* **10**, 25 (1989).

14. E.B. Dussan V and S.H. Davis, *J. Fluid Mech.* **65**, 71 (1974).

15. J.F. Oliver and S.G. Mason, *J. Colloid Interface Sci.* **60**, 480 (1977).

16. W.A. Zisman, *Adv. in Chem.* **43**, 1 (1964).

17. R.H. Dettre and R.E. Johnson, *Adv. in Chem.* **43**, 112 (1964).

18. E.B. Dussan V., *J. Fluid Mech.* **77**, 665 (1976).

19. W. B. Hardy, *Philos. Mag.* **38**, 49 (1919).

20. W. D. Bascom, R. L. Cottington and C. R. Singleterry, *Adv. in Chem.* **43**, 389 (1964).

21. W.A. Gross, L.A. Matsch, V. Castelli, A. Eshel, J.H. Vohr and M. Wildmann, *Fluid Film Lubrication*, (Wiley-Interscience, New York, 1980).

22. Fisher Scientific, Cat. no. G33.

23. Fisher Scientific, Cat. no. O122B.

24. Fisher Scientific, Cat. no. O121B.

25. Ref. (13) includes a calculation of the growth of small perturbations to the initially uniform front which predicts exponential growth at small times. Most of my data lie well outside this linear region.